SARS-CoV-2 sensing by RIG-I and MDA5 links epithelial infection to macrophage inflammation

Lucy G Thorne*[1+], Ann-Kathrin Reuschl*[1], Lorena Zuliani-Alvarez*[1], Matthew V.X. Whelan*[1], Mahdad Noursadeghi[1], Clare Jolly[§1+], Greg J Towers[§1+].

*, § These authors contributed equally. + Corresponding authors. 1. University College London, Division of Infection and Immunity, University College London, 90 Gower St, London WC1E 6BT, United Kingdom.

Graphical Abstract

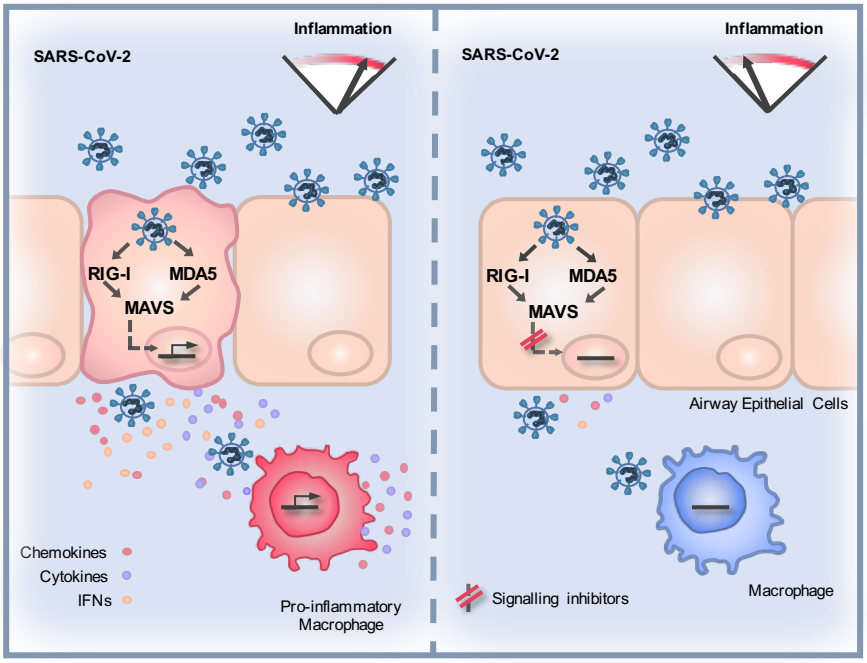

Highlights

- SARS-CoV-2 activates RNA sensors and consequent inflammatory responses in lung epithelial cells
- Epithelial RNA sensing responses drive pro-inflammatory macrophage activation
- Exogenous inflammatory stimuli exacerbate responses to SARS-CoV-2 in both eplithelial cells and macrophages
- Immunomodulators inhibit RNA sensing responses and consequent macrophage inflammation

Summary

SARS-CoV-2 infection causes broad-spectrum immunopathological disease, exacerbated by inflammatory co-morbidities. A better understanding of mechanisms underpinning virus-associated inflammation is required to develop effective therapeutics. Here we discover that SARS-CoV-2 replicates rapidly in lung epithelial cells despite triggering a robust innate immune response through activation of cytoplasmic RNA-sensors RIG-I and MDA5. The inflammatory mediators produced during epithelial cell infection can stimulate primary human macrophages to enhance cytokine production and drive cellular activation. Critically, this can be limited by abrogating RNA sensing, or by inhibiting downstream signalling pathways. SARS-CoV-2 further exacerbates the local inflammatory environment when macrophages or epithelial cells are primed with exogenous inflammatory stimuli. We propose that RNA sensing of SARS-CoV-2 in lung epithelium is a key driver of inflammation, the extent of which is influenced by the inflammatory state of the local environment, and that specific inhibition of innate immune pathways may beneficially mitigate inflammation-associated COVID-19.

Introduction

SARS-CoV-2 has caused a devastating pandemic, >74.8 million confirmed cases, >1.6 million deaths (https://covid19.who.int/, 20th December 2020) and a worldwide economic crisis. Infection causes a remarkably wide, but poorly understood, disease spectrum, ranging from asymptomatic (Allen et al., 2020;Treibel et al., 2020) to severe acute respiratory distress syndrome, multi-organ failure and death (Docherty et al., 2020;Zhou et al., 2020).

The success of immunosuppressive corticosteroid dexamethasone in treating COVID-19 (Beigel et al., 2020) suggests the importance of immunopathology in disease, likely driven by immune activation in infected and virus-exposed cells. Intracellular innate immune responses have evolved to detect and suppress invading pathogens, but inappropriate responses can also contribute to disease (Blanco-Melo et al., 2020;Park and Iwasaki, 2020). Pathogen associated molecular patterns (PAMPs) are detected by pattern recognition receptors (PRR), including cytoplasmic nucleic acid sensors, and Toll-like receptors (TLR) that sample extracellular and

endosomal space. PRR activation triggers signaling cascades which activate downstream transcription factors, including interferon (IFN) regulatory factors (IRFs) and NF-κB family members, to initiate a defensive pro-inflammatory gene expression programme, principally mediated by IFN secretion from infected cells. Paracrine and autocrine IFN signalling can suppress viral replication and spread and, together with other secreted cytokines and chemokines, coordinates adaptive immune responses. Viruses have evolved countermeasures to innate defences and deploy a combination of evasion, and direct innate immune pathway antagonism, to promote replication (Sumner et al., 2017). The resulting virus-host conflict is often a significant cause of pathogenesis with PRR-induced inflammation driving disease at the site of replication and systemically (Park and Iwasaki, 2020).

Missense mutations in innate immune pathways (Pairo-Castineira et al., 2020;Zhang et al., 2020), and autoantibodies leading to deficient Type 1 IFN responses (Bastard et al., 2020), are associated with severe COVID-19 suggesting that intact innate immune responses are important in preventing disease, probably through controlling viral replication. Co-morbidities linked to severe disease are typically inflammatory in nature suggesting that certain types of pre-existing inflammation influence disease severity (Paranjpe et al., 2020). However the specific host-pathogen interactions that cause disease, and how these are impacted by existing inflammation, are not understood. Identification of the molecular events that link viral replication to inflammation and disease will be critical in the development of novel and more precise therapeutic agents. Moreover, such new knowledge will provide insights into the mechanisms by which the associated risk factors for severe COVID-19 impact immune homeostasis in general.

Here we investigated early host-virus interactions to understand whether SARS-CoV-2 induces an innate response, whether it can escape consequent innate immune control and how it may propagate an immunopathogenic response. We focussed on lung epithelial cells and primary macrophages, which represent cells responsible for the earliest innate immune response to the virus (Bost et al., 2020;Chua et al., 2020). We found rapid replication and infectious virus release in lung epithelial cells prior to potent innate immune activation. Critically, the cocktail of soluble

mediators produced by infected cells strongly activated macrophages, which propagated a pro-inflammatory response. RNA sensing of infection by RIG-I and MDA5 was required for inducing the pro-inflammatory milieu as manipluation of the sensing events in epithelial cells, using RNA interference or signalling pathway inhibitors, dampened subsequent macrophage activation and inflammatory gene expression. Pre-exposure of epithelial cells or macrophages to exogenous inflammatory stimuli exacerbated inflammatory responses upon SARS-CoV-2 exposure. We propose that the innate immune microenvironment, in which sensing of SARS-CoV-2 infection occurs, determines the degree of virus-induced inflammation, and has the potential to drive disease.

Results

SARS-CoV-2 activates delayed innate immune responses in lung epithelial cells

In order to investigate innate immune responses to SARS-CoV-2, we first sought a producer cell line that did not respond to the virus, thereby allowing production of virus stocks free of inflammatory cytokines. As adaptive mutations have been reported during passage of the virus in Vero.E6 cells (Davidson et al., 2020;Ogando et al., 2020), we selected human gastrointestinal Caco-2 cells, which express the SARS-CoV-2 receptor ACE2 and entry factors TMPRSS2/4 (Figure S1A, B) and are naturally permissive (Stanifer et al., 2020). We found that Caco-2 support high levels of viral production (Figure S1C, D), but not virus spread (<15% cells infected) (Figure S1E, F). Importantly, they do not mount a detectable innate response to SARS-CoV-2 over 72 hpi at a range of multiplicities of infection (MOIs), as evidenced by a lack of inflammatory gene induction (Figure S1G) and undetectable cytokine secretion. They are also broadly less responsive to innate immune agonists than lung epithelial Calu-3 cells (compare Figure S1H-Caco-2 and S1I-Calu-3). Caco-2 cells were therefore used to produce SARS-CoV-2 stocks uncontaminated by inflammatory cytokines.

Comparatively, lung epithelial Calu-3 cells express high levels of receptor ACE2, and entry co-factors TMPRSS2 and TMPRSS4 (Figure S1A and B) (Hoffmann et al., 2020;Zang et al., 2020), and

are innate immune competent (Figure S1I) when stimulated with various PRR agonists. Consistently, Calu-3 cells supported very rapid spreading infection of SARS-CoV-2 followed by activation of innate immune responses. SARS-CoV-2 replication displayed >1000-fold increase in viral genomic and subgenomic (envelope, E) RNA levels within 5 hours post infection (hpi) across a range of MOIs 0.08, 0.4, 2 TCID50/cell (Figure 1A, Figure S2A), with TCID50 determined in Vero.E6 cells. Genomic and subgenomic E RNA in Calu-3 plateaued around 10 hpi. Rapid spreading infection was evidenced by increasing nucleocapsid protein (N)-positive cells by flow cytometry and immunofluorescence staining, peaking at 24 hpi with 50-60% infected cells (Figures 1B-D and Figure S2B). Infectious virus was evident in supernatants by 5 hpi at the highest MOI and peaked between 10-48 hpi, depending on MOI (Figure 1E, Figure S2C). A pronounced innate immune response to infection followed the peak of viral replication, evidenced by induction of cytokines (IL-6, TNF), chemokines (CCL2, CCL5) and type I and III IFNs (IFNβ, IFNλ1/3) measured by RT-qPCR (Figures 1F and G, and Figure S2D-F). This was accompanied by an IFN-stimulated gene (ISG) expression signature (CXCL10, IFIT1, IFIT2, MxA) (Figure 1H and Figure S2D-F). Gene induction was virus dose-dependent at 24 hpi, but equalised across all MOIs by 48 hpi, as the antiviral response to low-dose virus input maximised. These data show that infected lung epithelial cells can be a direct source of inflammatory mediators.

We were surprised that SARS-CoV-2 replicated so efficiently in Calu-3 despite innate immune responses including IFN and ISG expression because coronaviruses, including SARS-CoV-2 are reported to be IFN sensitive (Stanifer et al., 2020). Indeed, recombinant Type I IFN, but not type II or type III IFNs, effectively reduced SARS-CoV-2 infection if Calu-3 cells were treated prior to infection (Figure 1I-K, Figure S2G and H). However, Type I IFN had little effect on viral replication when added two hours after infection (Figure 1 I-K). Thus, the IFN response induced in infected lung epithelial Calu-3 cells appears too late to suppress SARS-CoV-2 replication in this system. To determine if viral exposure dose influences the race between viral replication and IFN, we infected cells at a 100x lower dose (MOI 0.0004 TCID50/cell) and observed a longer window of opportunity for exogenous Type I IFN to restrict viral replication (Figure 1 I-K). This is consistent with the hypothesis that high-dose infection can overcome IFN-inducible restriction.

Peak SARS-CoV-2 replication precedes innate immune activation

To understand the apparent disconnect in the kinetics between innate immune activation and viral replication, we used single-cell imaging to measure nuclear localisation of activated inflammatory transcription factors NF-κB p65 and IRF3, which mediate multiple PRR-signalling cascades. NF-κB p65 nuclear translocation coincided with cells becoming N protein positive and a change was evident from 5 hpi (Figure 2A and B, Figure S3A). The timing of NF-κB p65 translocation was dependant on the viral dose, from 5 hpi for the highest MOI (2 TCID50/cell, Figure S3), between 5 - 10 hpi for MOIs 0.4 and 0.04 (Figures 2A and B, Figure S3), and 24 – 48 hpi for MOI 0.004 (Figure S3). IRF3 activation was also virus dose dependent but did not maximise until 72 hpi, later than NF-κB (Figures 2C and D, Figure S3). These data are consistent with the requirement of a threshold of viral RNA replication to induce transcription factor translocation, particularly for IRF3, and innate immune activation. Although small variation in NF-κB p65 and IRF3 nuclear intensity was observed in N negative cells, we did not see the same large increases sustained throughout the timecourse as in N positive cells, consistent with direct activation of NF-κB p65 and IRF3 by virus replication (Figure S3).

Supporting the observation of activation of NF-κB p65 and IRF3 activation by SARS-CoV-2 infection, single cell fluorescence *in situ* hybridisation (FISH) analysis of IL-6 mRNA (a prototypic NF-κB regulated cytokine), showed increased IL-6 transcripts uniquely in N-positive infected cells, appearing at 6 hpi and peaking at 24hpi (Figure 2E and F, Figure S4A). IFIT1 transcripts (a prototypic ISG) measured by FISH also demonstrated rapid induction in N-positive cells with increased signal from at 6 hpi (Figure 2H). Strikingly, IFIT1 mRNA was not highly induced in N-negative bystander cells consistent with defective interferon responses failing to induce ISGs and a timely antiviral state in uninfected cells (Figure 2H). As a control for these changes, we show that GAPDH transcripts did not change (Figure S4B). Secretion of pro-inflammatory chemokine CXCL10, and cytokine IL-6, followed gene expression and were detected from 24 hpi (Figure 2I and J, Figure S4C). Further analysis revealed increases in lactate dehydrogenase (LDH) in infected cell supernatants from 48 hpi, equal across all MOIs, indicative of pro-inflammatory cell death

(Figure 2K, S4D). Importantly cytokine secretion had also equalised across MOIs from 24 hpi (Figure 2I and J). LDH release paralleled loss of the epithelial monolayer integrity (Figure 1C) and cell death (Figure 2L, Figure S4E and F) accounting for the reduction in cytokine secretion at 72 hpi (Figures 2I and J).

SARS-CoV-2 is sensed by MDA5 and RIG-I

To determine the mechanism of virus sensing by innate pathways, we first confirmed that viral RNA replication is required for innate immune activation. Inhibition of viral RNA replication, with polymerase inhibitor Remdesivir, abrogated pro-inflammatory and ISG gene expression in a dose-dependent manner (Figure 3A-D). Critically, Remdesivir was only effective if added prior to, or at the time of infection, consistent with a requirement for metabolism to its active tri-phosphorlyated form (Eastman et al., 2020) (Figures 3 E-H).

Inflammatory gene induction dependent on viral genome replication suggested that an RNA sensor activates this innate response. Both genomic and subgenomic SARS-CoV-2 RNAs are replicated via double stranded intermediates in the cytoplasm (Li et al., 2020). Accordingly, we detected cytoplasmic dsRNA at 5 hpi in Calu-3 cells, preceding N positivity (Figure 3I) and by 48 hpi all dsRNA positive cells were N positive. Depletion of RNA sensing adaptor MAVS abolished SARS-CoV-2-induced IL-6, CXCL10, IFNβ and IFIT2 gene expression (Figures 3 J-N), consistent with RNA sensing being a key driver of SARS-CoV-2-induced innate immune activation. Concordantly, depletion of cytoplasmic RNA sensors RIG-I or MDA-5 also reduced inflammatory gene expression after infection (Figures 3J-N). This suggested sensing of multiple RNA-species given the different specificities of RIG-I and MDA5 (Hornung et al., 2006;Kato et al., 2006;Rehwinkel et al., 2010;Wu et al., 2013). Intriguingly, unlike RIG-I, MDA5 was not required for induction of IL-6 mRNA, consistent with differences in downstream consequences of RIG-I and MDA5 activation (Figure 3M) (Brisse and Ly, 2019). Abrogating SARS-CoV-2 sensing via MDA5 and MAVS depletion also reduced cell death, suggesting cell death is mediated by the host response rather than direct virus-induced damage (Figure 3O). Notably, sensor depletion did not strongly increase viral RNA

levels (Figure 3P), or the amount of released infectious virus (Figure 3Q), confirming that innate immune activation via RNA sensing did not potently inhibit viral replication.

NF-κB and JAK/STAT signalling drive innate immune responses

As a complementary approach to mapping SARS-CoV-2-induced innate immune activation, and to assess the potential of specific immunomodulators to impact inflammatory responses and viral replication, we examined the effect of inhibiting NF-κB activation using IK-β kinase (IKK-β) inhibitors TPCA-1 and PS1145. IKK-β is responsible for NF-κB p65 activation by phosphorylation following PRR signalling. Induction of ISGs and IL-6 was inhibited by TPCA-1, and with slightly reduced potency PS1145 (Figure 4A-C, Figure S5A and B). Inhibiting Janus kinase (JAK) with Ruxolitinib, to prevent JAK signalling downstream of the Type I IFN receptor (IFNAR), also suppressed SARS-CoV-2 induced ISGs, but not NF-κB-sensitive IL-6 (Figure 4D-F and Figure S5C). Neither TPCA-1 nor Ruxolitinib treatment increased viral genome replication over a wide range of MOIs (Figure 4G and H) or N positivity or virion production after single dose infection (Figure S5D-F). Importantly, NF-κB and JAK inhibition significantly reduced cell death in infected cultures (Figure 4I). This is consistent with our earlier observation and with the notion that the innate immune response to infection is the main driver of lung epithelial cell damage. Our data thus far, show that SARS-CoV-2 infection of Calu-3 lung epithelial cells results in multi-pathway activation, driving pro-inflammatory and IFN-mediated innate immune responses that are inadequate or arise too late to restrict virus. Critically, they also suggest that SARS-CoV-2 induced IFN and pro-inflammatory gene expression can be therapeutically uncoupled from viral replication.

Epithelial responses to SARS-CoV-2 drive macrophage activation

Resident and recruited pro-inflammatory macrophages in the lungs are associated with severe COVID-19 disease (Bost et al., 2020;Liao et al., 2020;Pairo-Castineira et al., 2020;Szabo et al., 2020). We therefore asked whether macrophages can support SARS-CoV-2 infection and how they respond indirectly to infection, through exposure to conditioned medium from infected epithelial cells. Importantly, neither primary monocyte-derived macrophages (MDM), nor PMA-differentiated THP-1 cells (as an alternative macrophage model), supported SARS-CoV-2

replication, evidenced by lack of increase in viral RNA and by the absence of N positive cells (Figures S6A-C). This is consistent with their lack of ACE2 and TMPRSS2 expression (Figure S1A, B). However, exposure of MDM to virus-containing conditioned medium from infected Calu-3 cells (Figure 5A) led to significant macrophage ISG induction (Figure 5B, E, H) and increased expression of macrophage-activation markers CD86 and HLA-DR (Figure 5C-D, F-G, I-J). Importantly, the immune stimulatory activity of conditioned media was dependent on RNA sensing and innate immune activation in infected Calu-3 cells because induction of inflammatory genes and macrophage activation markers was abolished by depletion of MAVS prior to Calu-3 infection (Figure 5B-D) or by inhibition of NF-κB (TPCA-1) or JAK activation (Ruxolitinib) in infected Calu-3 (Figure 5E-J). Note that in these experiments, MDM were exposed to equivalent numbers of viral genomes from the MAVS depleted, or inhibitor treated conditioned media (Figure S6D-F). These data demonstrate that production of inflammatory mediators from infected lung epithelial cells, downstream of viral RNA sensing, can propagate pro-inflammatory macrophage activation.

Pre-existing immune activation exacerbates SARS-CoV-2-dependent inflammation

Severe COVID-19 is associated with inflammatory co-morbidities suggesting that pre-existing inflammatory states lead to inappropriate immune responses to SARS-CoV-2 and drive disease (Lucas et al., 2020;Mehra et al., 2020;Williamson et al., 2020;Wolff et al., 2020;Zhang et al., 2020). Macrophages in particular are thought to potentiate inflammatory responses in the lungs of severe COVID-19 patients (Nicholls et al., 2003;Liao et al., 2020) and so we investigated whether inflammatory stimuli might directly exacerbate macrophage responses to SARS-CoV-2 alone (Figure 6A-H). In these experiments we produced virus in Caco-2 and therefore it did not contain inflammatory cytokines (Figure S1G). We detected low level innate immune activation after exposure of MDM to SARS-CoV-2 alone (Figure 6B-H). However, when MDM were primed with 100 ng/ml LPS prior to exposure to SARS-CoV-2, we observed an enhanced response compared to exposure to virus or LPS alone, evidenced by significantly increased levels of ISGs (Figure 6D and E) and pro-inflammatory CCL5 (Figure 6C). Of note, LPS alone induced IL-6 and inflammasome-associated IL-1β expression and secretion and this was unaffected by virus

exposure (Figure 6F-H). Exposure of MDM to SARS-CoV-2, prior to stimulation with LPS (Figure 6I-P), also enhanced macrophage inflammatory and ISG responses, but not IL-6 or IL-1β expression and secretion, compared to those detected with virus or LPS alone (Figure 6J-P). LPS treatment of MDM before or after virus challenge did not induce SARS-CoV-2 permissivity, evidenced by failure to increase the level of detectable viral E gene in MDM supernatants (Figure 6B and J).

Finally, we modelled the lung epithelial cell response to the cytokines observed in activated macrophages. We first selected IL-1β, as it was produced by LPS-treated, LPS-primed virus-exposed and virus primed LPS-exposed MDM (Figure 6G and H, O and P) and has been observed in severe COVID-19 patient lungs (Laing et al., 2020;Rodrigues et al., 2021). Treatment of Calu-3 with IL-1β during infection significantly increased induction of both ISGs and pro-inflammatory cytokines, compared to their induction by virus alone (Figure 6Q-T). The exception was IL-6, which was highly induced by virus even in the absence of IL-1β pre-treatment (Figure 6S). Next we treated Calu-3 cells with TNF, which is also produced by LPS-treated or primed MDM (Figure S7A and B) and implicated in severe COVID-19 (Chua et al., 2020;Mahase, 2020), but found no enhancement of innate responses to SARS-CoV-2 (Figure S7C). However, both IL-1β and TNF treatment increased virus-induced epithelial cell death (Figure 6U and Figure S7D), without impacting viral replication (Figure 6V and Figure S7E). Together, these data suggest that SARS-CoV-2 infection of lung epithelium can promote immune activation of inflammatory macrophages, via secretion of cytokines, chemokines and virus from infected cells, and that this can be exacerbated by a pre-existing pro-inflammatory state. This is consistent with the hypothesis that chronic inflammatory states, rather than enhanced viral replication, drive detrimental immune activation and/or cell death.

Discussion

We found that SARS-CoV-2 can replicate and spread effectively in lung epithelial Calu-3 cells over a wide range of inoculum doses despite inducing potent IFN responses and ISG expression. We

propose that in the model system used here, innate immune activation occurs too late to suppress replication and attribute this to the virus deploying innate immune evasion and antagonism strategies early in infection. Indeed, coronaviruses replicate inside membranous vesicles, thought to protect viral RNA species from cytoplasmic sensing, and have complex capacity to antagonise innate immunity, including inhibition of MDA5 activation (Liu et al., 2020) and preventing nuclear entry of inflammatory transcription factors (Totura and Baric, 2012;Banerjee et al., 2020;Miorin et al., 2020;Park and Iwasaki, 2020;Yuen et al., 2020). Indeed, it is possible that the innate immune response and the secreted signals produced by infected cells are dysregulated by viral manipulation, and that this imbalanced response may also contribute to disease when occurring during underlying inflammatory pathology (Blanco-Melo et al., 2020;Giamarellos-Bourboulis et al., 2020;Lucas et al., 2020).

We demonstrate that SARS-CoV-2 can be sensed by both RIG-I and MDA5 and that, through their signalling adaptor MAVS, these sensors drive inflammatory responses in infected Calu-3 cells. Concordantly, both RIG-I and MDA5 have been implicated in sensing the murine coronavirus mouse hepatitis virus (Roth-Cross et al., 2008;Li et al., 2010) and MDA5 was recently shown to sense SARS-CoV-2 and trigger IFN production (Rebendenne et al., 2020). Likewise, activation of dsRNA sensor PKR has also been observed during SARS-CoV-2 infection of other cell types (Li et al., 2020). The eventual innate immune activation in Calu-3 cells is likely due to sensing of viral RNA when it accumulates to a level that overcomes sequestration and pathway inhibition by the virus, as well as to cellular stress responses to infection. Importantly, Calu-3 cells pre-treated with IFN resist infection illustrating that innate responses can suppress SARS-CoV-2 replication if an antiviral state is induced prior to infection, particularly with a low viral exposure dose.

Although SARS-CoV-2 RNA has been found associated with macrophages and monocytes from infected patients (Bost et al., 2020), we found that macrophage did not support SARS-CoV-2 replication. However, they were sensitive to conditioned media from infected Calu-3 containing virus, IFNs and pro-inflammatory mediators, inducing high levels of chemokine and ISG mRNA and expression of activation markers CD86 and HLA-DR upon exposure. Crucially, it is the

response of the Calu-3 cells to virus infection, via RNA sensing, that drives macrophage activation in these experiments, evidenced by suppression of activation after either MAVS depletion or NF-κB (TPCA-1) or JAK inhibition (Ruxolitinib) in the infected Calu-3 cells. Importantly, inhibiting RNA sensing or pathway activation did not particularly increase viral replication, consistent with our observation that, in this model at least, virus-induced innate immune responses do not significantly inhibit SARS-CoV-2 replication. These observations highlight the potential of immunomodulators in reducing SARS-CoV-2 driven inflammatory disease. Indeed, suppression of JAK1/2 signalling with Baricitinib, in SARS-CoV-2 infected macaques, significantly reduced macrophage recruitment and inflammatory signatures and preliminary data support its use in COVID-19 (Bronte et al., 2020). These studies are consistent with epithelial-driven inflammation contributing to myeloid cell infiltration and the role of macrophages in exacerbating immune responses in COVID-19 (Giamarellos-Bourboulis et al., 2020;Hoang et al., 2020;Liao et al., 2020). Our data provide a framework for dissecting immunomodulators as therapeutics and we propose that it is essential to test both immunomodulators, and direct acting antivirals, in innate-immune competent cells, rather than in Caco-2, Vero or other innate immune-inactive cell types, because the inevitable interactions between virus replication and innate immune pathways can influence drug efficacy and potency (Rasaiyaah et al., 2013;Kim et al., 2019;Sumner et al., 2020).

A key question is how our experiments in Calu-3 cells inform understanding of COVID-19. We propose that by studying virus replication in innate immune competent permissive host cells we can probe the earliest interactions between the virus and the host that underpin subsequent inflammatory responses. Our data show that RNA sensing in infected Calu-3 cells creates a pro-inflammatory milieu capable of activating primary macrophages. Crucially the combined profile of pro-inflammatory mediators in this system mirrors that observed in COVID-19 *in vivo* (Bost et al., 2020;Laing et al., 2020;Szabo et al., 2020). We propose that *in vivo* it is the innate immune microenvironment in which the virus-host interaction occurs, and its consequent influence on immune activation, that determines disease outcome. This is consistent with our demonstration that exogenous inflammatory stimuli can drive a state in Calu-3 cells, and primary macrophages, that influences the response to virus, exacerbating inflammation. This link, between the

immediate epithelial response to infection and external inflammatory signals, both amplified by macrophages, provides a plausible hypothesis to explain the association of severe COVID-19 with the presence of proinflammatory macrophages in broncheoalvolar lavage and patient lungs (Giamarellos-Bourboulis et al., 2020;Liao et al., 2020;Szabo et al., 2020) and inflammatory co-morbidities (Mehra et al., 2020;Williamson et al., 2020;Wolff et al., 2020), which could provide similar inflammatory stimulation.

It is remarkable how effective SARS-CoV-2 is in escaping human innate immune responses at the cellular level, despite being a recent zoonosis. Very low levels of adaptive change are consistent with adaptation to human replication prior to identification. Whether SARS-CoV-2 adapted in a non-human species prior to human infection, or whether adaptation in humans occurred before identification, remains unclear. One possibility is that coronaviruses replicate in a conserved niche, with regard to innate immune evasion, and thus are particularly good at zoonosis, perhaps evidenced by SARS-CoV-2 being preceded by SARS-CoV-1 and Middle Eastern Respiratory Syndrome virus (MERS), and apparent cross species transfer and transmission in distantly related species including humans, bats (Boni et al., 2020), camels (Azhar et al., 2014), civet cats (Wang and Eaton, 2007) and mink (Koopmans, 2020).

Viral disease is often driven by host immune mechanisms that have evolved to protect the host from death, a paradox that is particularly evident in COVID-19. Here we have taken a significant step towards explaining the consequences of SARS-CoV-2 infection of innate immune competent lung epithelial cells by illustrating how RNA sensing can drive potent inflammatory responses, irrespective of whether virus replication is suppressed. We propose that further studies addressing mechanisms of SARS-CoV-2 immune evasion and cytopathology, and the wider impact these have on epithelial-immune cell cross-talk, will inform development of effective therapeutics that are broadly active against zoonotic coronaviruses.

Methods

Cell culture and innate immune stimulation

Calu-3 cells (ATCC HTB-55) and Caco-2 cells were a kind gift Dr Dalan Bailey (Pirbright Institute). THP-1 Dual cells were obtained from Invivogen. Vero.E6 were provided by NIBSC, Beas2B (ATCC CRL-9609) and Hulec5a (ATCC CRL-3244) were obtained from ATCC, and Detroit 562 (ATCC CCL-138) were a kind gift from Dr Caroline Weight (UCL). All cells except THP-1 were cultured in Dulbecco's modified Eagle Medium (DMEM) supplemented with 10% heat-inactivated FBS (Labtech), 100U/ml penicillin/streptomycin, with the addition of 1% Sodium Pyruvate (Gibco) and 1% Glutamax for Calu-3 and Caco-2 cells. All cells were passaged at 80% confluence. For infections, adherent cells were trypsinised, washed once in fresh medium and passed through a 70 µm cell strainer before seeding at 0.2x10^6 cells/ml into tissue-culture plates. Calu-3 cells were grown to 60-80% confluence prior to infection. THP-1 cells were cultured in RPMI (Gibco) supplemented with 10 % heat-inactivated FBS (Labtech), 100U/ml penicillin/streptomycin (Gibco), 25 mM HEPES (Sigma), 10 µg/ml of blasticidin (Invivogen) and 100 µg/ml of Zeocin™ (Invivogen).Caco-2 and Calu-3 cells were stimulated for 24 h with media containing TLR4 agonist Lipopolysaccharide (LPS) (Peprotech), the TLR3 agonist poly I:C (Peprotech) or the TLR7 agonist R837 (Invivogen), using the concentration stated on each figure. To stimulate RIG-I/MDA5 activation in Calu-3 cells, poly I:C was transfected. Transfection mixes were prepared using lipofectamine 2000 (Invitrogen) in Optimem (Thermofisher Scientific) according to the manufacturer's instructions.

Isolation of primary monocyte-derived macrophages

Primary monocyte-derived macrophages (MDM) were prepared from fresh blood from healthy volunteers. The study was approved by the joint University College London/University College London Hospitals NHS Trust Human Research Ethics Committee and written informed consent was obtained from all participants. Peripheral blood mononuclear cells (PBMCs) were isolated by density gradient centrifugation using Lymphoprep (Stemcell Technologies). PBMCs were washed three times with PBS and plated to select for adherent cells. Non-adherent cells were washed away after 2 h and the remaining cells incubated in RPMI (Gibco) supplemented with 10 % heat-inactivated pooled human serum (Sigma) and 100 ng/ml macrophage colony stimulating factor (Peprotech). The medium was replaced after 3 days with RPMI with 5% FCS, removing any

remaining non-adherent cells. Cells were infected or treated with conditioned media 3-4 days later.

Virus culture and infection

SARS-CoV-2 strain BetaCoV/Australia/VIC01/2020 (NIBSC) was propagated by infecting Caco-2 cells at MOI 0.01 TCID50/cell, in DMEM supplemented with 2% FBS at 37°C. Virus was harvested at 72 hours post infection (hpi) and clarified by centrifugation at 4000 rpm for 15 min at 4 °C to remove any cellular debris. Virus stocks were aliquoted and stored at -80 °C. Virus titres were determined by 50% tissue culture infectious dose (TCID50) on Vero.E6 cells. In brief, 96 well plates were seeded at 1x10^4 cells/well in 100 µl. Eight ten-fold serial dilutions of each virus stock or supernatant were prepared and 50 µl added to 4 replicate wells. Cytopathic effect (CPE) was scored at 5 days post infection, and TCID50/ml was calculated using the Reed & Muench method (Reed, 1938), and an Excel spreadsheet created by Dr. Brett D. Lindenbach was used for calculating TCID50/mL values (Lindenbach, 2009).

For infections, multiplicities of infection (MOI) were calculated using TCID50/cell determining on Vero.E6 cells. Cells were inoculated with diluted virus stocks for 2h at 37 °C. Cells were subsequently washed twice with PBS and fresh culture medium was added. At indicated time points, cells were harvested for analysis.

MDM were infected with virus diluted in RPMI, 5% FBS (estimated MOI 0.02 TCID50/cell). MDM were harvested at 24h or 48 hpi for gene expression analysis. For priming experiments, MDM were stimulated with 100 ng/mL of LPS (HC4046, Hycult Biotech) for 2h. Media was replaced and cells were exposed to SARS-CoV-2 as before, diluted in RPMI, 5% FBS. Cells were collected after 48h for analysis. Alternatively, cells were mock exposed or exposed to SARS-CoV-2 for 3 days and then stimulated with 100 ng/mL of LPS. Cells were harvested after 24h for analysis.

Sensor and adaptor depletion by RNAi

Calu-3 cells were transfected with 40 pmol of siRNA SMART pool against RIG-I (L-012511-00-0005), MDA5 (L-013041-00-0005), MAVS (L-024237-00-0005) or non-targeting control (D-

001810-10-05) (Dharmacon) using Lipofectamine *RNAiMAX* Transfection Reagent (Invitrogen). Transfection medium was replaced after 24h with DMEM medium supplemented with 10% FBS, 100U/ml penicillin/streptomycin and cells cultured for additional 2 days. On day 3, cells were transfected again with the same siRNA smart pools. Transfection medium was replaced after 24h and cells cultured for additional 2 days before infection. Gene depletion was verified using TaqMan Gene Expression Assay according to manufacturer's instructions detecting human RIG-I (FAM dye-labelled, TaqMan probe ID no. Hs01061436_m1), MAVS (FAM dye-labelled, TaqMan probe ID no. Hs00920075_m1), MDA5 (FAM dye-labelled, TaqMan probe ID no. Hs00223420_m1) or the housekeeping gene OAZ1 (FAM dye-labelled, TaqMan probe ID no. Hs00427923_m1)

Treatment with cytokines, inhibitors and conditioned medium

Calu-3 cells were pre-treated with Remdesivir (Selleck Chemicals), TPCA-1 (Biotechne), PS-1145 (BioTechne) or Ruxolitinib (Biotechne) at the indicated concentrations or DMSO control at an equivalent dilution for 1 h before SARS-CoV-2 infection unless otherwise stated. Inhibitors were maintained at the indicated concentrations throughout the experiments. For cytokine treatments, recombinant human IFNβ, IFNλ1, IFNλ2, IFNγ, IL1β or TNF (Peprotech) at a final concentration of 10 ng/ml were added at the indicated time points. To generate conditioned media (CoM), Calu-3 cells were mock-infected or infected with SARS-CoV-2 at 0.04 TCID50/cell and supernatants were harvested 48 hpi, clarified by centrifugation at 4000 rpm for 15 minutes and 4 °C and stored at -80 °C. For conditioned media experiments, MDM were exposed to CoM as indicated, which was diluted 1:5 in RPMI, 5% FBS. After 6 hours, conditioned medium was replaced with RPMI, 5% FBS and cells were harvested at 48 h for gene expression and surface marker expression analysis.

qRT-PCR

RNA was extracted using RNeasy Micro Kits (Qiagen) and residual genomic DNA was removed from RNA samples by on-column DNAse I treatment (Qiagen). Both steps were performed according to the manufacturer's instructions. cDNA was synthesized using SuperScript III with random hexamer primers (Invitrogen). qRT-PCR was performed using Fast SYBR Green Master

Mix (Thermo Fisher) for host gene expression or TaqMan Master mix (Thermo Fisher) for viral RNA quantification, and reactions performed on the QuantStudio 5 Real-Time PCR systems (Thermo Fisher). Host gene expression was determined using the 2-ΔΔCt method and normalised to GAPDH expression. Viral RNA copies were deduced by standard curve, using primers and a Taqman probe specific for E, as described elsewhere (Corman et al., 2020) and below.

The following primers and probes were used:

Target	Sequence
ACE2	Fwd 5'-CGAAGCCGAAGACCTGTTCTA -3' Rev 5'-GGGCAAGTGTGGACTGTTC-3'
CCL5	Fwd: 5'-CCCAGCAGTCGTCTTTGTCA-3' Rev 5'- TCCCGAACCCATTTCTTCTCT-3'
CXCL10	Fwd 5'-TGGCATTCAAGGAGTACCTC-3' Rev 5'-TTGTAGCAATGATCTCAACACG-3'
GAPDH	Fwd 5'-GGGAAACTGTGGCGTGAT-3' Rev 5'-GGAGGAGTGGGTGTCGCTGTT-3'
IFIT1	Fwd 5'-CCTCCTTGGGTTCGTCTACA-3' Rev 5'-GGCTGATATCTGGGTGCCTA-3'
IFIT2	Fwd 5'-CAGCTGAGAATTGCACTGCAA-3' Rev 5'-CGTAGGCTGCTCTCCAAGGA-3'
IFNB1	Fwd 5'-AGGACAGGATGAACTTTGAC-3' Rev 5'-TGATAGACATTAGCCAGGAG-3'
IFNL1	Fwd 5'-CACATTGGCAGGTTCAAATCTCT-3' Rev 5'- CCAGCGGACTCCTTTTTGG-3'
IFNL3	Fwd 5'- TAAGAGGGCCAAAGATGCCTT-3' Rev 5'- CTGGTCCAAGACATCCCCC-3'
IL1B	Fwd: 5'- CCTCCTTGGGTTCGTCTACA-3' Rev 5'-GGCTGATATCTGGGTGCCTA-3'
IL6	Fwd 5'-AAATTCGGTACATCCTCGACG-3' Rev 5'-GGAAGGTTCAGGTTGTTTTCT-3'
MX1	Fwd 5'-ATCCTGGGATTTTGGGGCTT-3' Rev 5'-CCGCTTGTCGCTGGTGTCG-3'
TMPRSS2	Fwd 5'-CAAGTGCTCCAACTCTGGGAT -3' Rev 5'-AACACACCGATTCTCGTCCTC-3'
TMPRSS4	Fwd 5'-ATGCGGAACTCAAGTGGGC-3' Rev 5'-CTGTTTGTCGTACTGGATGCT-3'
TNF	Fwd 5'-AGCCTCTTCTCCTTCCTGATCGTG-3' Rev 5'-GGCTGATTAGAGAGAGGTCCCTGG-3'

SARS-CoV-2 E_Sarbeco_F	5'-ACAGGTACGTTAATAGTTAATAGCGT-3'
SARS-CoV-2 E_Sarbeco_Probe1	5'-FAM-ACACTAGCCATCCTTACTGCGCTTCG-TAMRA-3'
SARS-CoV-2 E_Sarbeco_R	5'-ATATTGCAGCAGTACGCACACA-3'

Cytokine and LDH measurement

Secreted mediators were detected in cell culture supernatants by ELISA. CXCL10 and IL6 protein were measured using Duoset ELISA reagents (R&D Biosystems) according to the manufacturer's instructions.

Secreted lactate dehydrogenase (LDH) activity was measured as a correlate of cell death in culture supernatants using Cytotoxicity Detection Kit^{PLUS} (Sigma) according to the manufacturer's instructions. Culture supernatants were collected at the indicated time points post infection, clarified by centrifugation and stored at 4 °C until LDH measurement.

Flowcytometry

For flowcytometry analysis, adherent cells were recovered by trypsinising or gentle scraping and washed in PBS with 2mM EDTA (PBS/EDTA). Non-adherent cells were recovered from culture supernatants by centrifugation for 5 min at 1600 rpm and washed once in PBS/EDTA. Cells were stained with fixable Zombie UV Live/Dead dye (Biolegend) for 6 min at room temperature. Excess stain was quenched with FBS-complemented DMEM. For MDMs, Fc-blocking was performed with PBS/EDTA+10% human serum for 10 min at 4˚C. Cell surface with CD86-Bv711 (IT2.2, Biolegend) and HLA-DR-PerCpCy5.5 (L243, Biolegend) staining was performed in PBS/EDTA at 4˚C for 30min. Unbound antibody was washed off thoroughly and cells were fixed in 4% PFA prior to intracellular staining. For intracellular detection of SARS-CoV-2 nucleoprotein, cells were permeabilised for 15 min with Intracellular Staining Perm Wash Buffer (BioLegend). Cells were then incubated with 1µg/ml CR3009 SARS-CoV-2 cross-reactive antibody (a kind gift from Dr. Laura McCoy,) in permeabilisation buffer for 30 min at room temperature, washed once and incubated with secondary Alexa Fluor 488-Donkey-anti-Human IgG (Jackson Labs). All samples were acquired on

a BD Fortessa X20 or LSR II using BD FACSDiva software. Data was analysed using FlowJo v10 (Tree Star).

Western blotting

For detection of ACE2 expression, whole cell protein lysates were separated by SDS-PAGE, transferred onto nitrocellulose and blocked in PBS with 0.05% Tween 20 and 5% skimmed milk. Membranes were probed with polyclonal goat anti-human ACE2 (1:500, AF933, R&D Biosystems) or rabbit anti-human beat-Actin (1:2500, 6L12, Sigma) followed by donkey anti-goat IRdye 680CW or goat anti-rabbit IRdye 800CW (Abcam), respectively. Blots were Imaged using an Odyssey Infrared Imager (LI-COR Biosciences) and analysed with Image Studio Lite software.

Immunofluorescence microscopy and RNA-fluorescent *in situ* hybridization

For imaging analysis, Calu-3 or Caco-2 cells were seeded and infected with SARS-CoV-2 in Optical 96-well plates (CellCarrier Ultra, PerkinElmer) and cells were fixed with 4% PFA at the indicated timepoints. Permeabilisation was carried out with 0.1% TRITON-X100 (Sigma) in PBS for 15 minutes. A blocking step was carried out for 1h at room temperature with 10% goat serum/1%BSA in PBS. Nucleocapsid (N) proten detection was performed by primary incubation with human anti-N antibody (Cr3009, 1ug/ml) for 18h, and washed thoroughly in PBS. Where appropriate, N-protein staining was followed by incubation with rabbit anti-NFkB (p65) (sc-372, Santa Cruz) or rabbit anti-IRF3 (sc-9082, Santa Cruz) for 1 h. Primary antibodies were detected by labelling with with secondary anti-human AlexaFluor488 and anti-rabbit AlexaFluor546 conjugates (Jackson Immuno Research) for 1h. For RNA fluorescent *in situ* hybridization **(**FISH), cells were immunofluorescently labelled for viral N-protein (detected with AlexaFluor488 or AlexaFluor546 conjugates) followed by RNA visualisation using the ViewRNA Cell Plus Kit (Thermo Fisher). The ViewRNA probes implemented targeted *IL-6* (VA4-19075, AlexaFluor488), *IFIT1* (VA4-18833, AlexaFluor488) and *GAPDH* (VA1-10119, AlexaFluor546). All cells were then labelled with HCS CellMask DeepRed (H32721, Thermo Fisher) and Hoechst33342 (H3570, Thermo Fisher). Images were acquired using the WiScan® Hermes High-Content Imaging System (IDEA Bio-medical, Rehovot, Israel) at magnification 10X/0.4NA or 40X/0.75NA. Four channel automated acquisition was carried out sequentially (DAPI/TRITC, GFP/Cy5). For 10X magnification 100%

density/100% well area was acquired, resulting in 64 FOV/well. For 40X magnification, 35% density/ 30% well area was acquired resulting in 102 FOV/well.

Image analysis

NF-κB, IRF3, *IL6* and *GAPDH* raw image channels were pre-processed using a batch rolling ball background correction in FIJI imagej software package (Schindelin et al., 2012) prior to quantification. Automated image analysis was carried out using the 'Athena' HCS analysis software package (IDEA Bio-medical IDEA Bio-medical, Rehovot, Israel). For quantification of the percentage of nucleocapsid positive cells within the population, the 'Intracellular Granules' module was utilised. Nuclei were segmented using Hoechst33342 signal. Cell boundaries were determined by segmentation of CellMask signal. Infected cells were determined by thresholding intracellular N protein signal (Intracellular granules). For all analysis, the N protein signal intensity was thresholded against the mock infected wells to ensure no false segmentation of N +ve objects. Nuclear accumulation of NF-κB or IRF3 was carried out using the 'Intranuclear Foci' module. Nuclei of cells were segmented using the Hoechst33342 stain. 'Foci' of perinuclear N protein signal were identified and an 'Infected' cell population determined based on the presence of such segmented foci objects. In all cells the NF-κB or IRF3 signal present within segmented nuclei was quantified. For RNA-FISH quantification the 'Mitochondria' module was implemented. Nuclei were segmented using the Hoechst33342 stain. Cell cytoplasmic area was determined by segmentation of CellMask 647 signal. Intracellular N protein signal was segmented as 'mitochondria' objects. *IL-6*/*GAPDH* RNA FISH signal within segmented cells was then quantified. Infected cells were determined by the presence of N protein segmented objects within the cell. Analysis parameters are detailed in Supplementary Table 1A-C.

Statistical analysis

Statistical analysis was performed using GraphPad Prism. As indicated, normally distributed data was analysed for statistical significance by *t*- tests (when comparing two groups) or one-way ANOVA with Bonferroni or Dunnett's post-test (when comparing more than two groups). Wilcoxon ranked paired non-parametric tests were performed for primary macrophage data that

was not normally distributed. For imaging analysis, where appropriate, integrated intensities were normalised to the mean intensity of the mock infected population for that respective timepoint. Comparisons were made using a Kruskal-Wallis test with Dunn's multiple comparison. Data show the mean +/- the S.E.M, where appropriate the median is shown, with significance shown on the figures, levels were defined as *, $P < 0.05$; **, $P < 0.01$ and ***, $P < 0.001$, ****, $P < 0.0001$.

Acknowledgements

MN and CJ were funded by Wellcome Investigator Awards, and GJT was funded by a Wellcome Senior Fellowship. Funds were also obtained from the University College London COVID-19 fund and the National Institutes of Health Research UCL/UCLH Biomedical Research Centre. We are grateful to Giada Mattiuzzo at NIBSC for SARS-CoV-2 and reagents, Laura McCoy at UCL for SARS-CoV-2 N antibody, Dalan Bailey at The Pirbright Institute and Richard Milne at UCL for valuable discussions and critical reading of the manuscript.

References

Allen, W.E., Altae-Tran, H., Briggs, J., Jin, X., Mcgee, G., Shi, A., Raghavan, R., Kamariza, M., Nova, N., Pereta, A., Danford, C., Kamel, A., Gothe, P., Milam, E., Aurambault, J., Primke, T., Li, W., Inkenbrandt, J., Huynh, T., Chen, E., Lee, C., Croatto, M., Bentley, H., Lu, W., Murray, R., Travassos, M., Coull, B.A., Openshaw, J., Greene, C.S., Shalem, O., King, G., Probasco, R., Cheng, D.R., Silbermann, B., Zhang, F., and Lin, X. (2020). Population-scale longitudinal mapping of COVID-19 symptoms, behaviour and testing. *Nat Hum Behav* 4**,** 972-982.

Azhar, E.I., El-Kafrawy, S.A., Farraj, S.A., Hassan, A.M., Al-Saeed, M.S., Hashem, A.M., and Madani, T.A. (2014). Evidence for camel-to-human transmission of MERS coronavirus. *N Engl J Med* 370**,** 2499-2505.

Banerjee, A.K., Blanco, M.R., Bruce, E.A., Honson, D.D., Chen, L.M., Chow, A., Bhat, P., Ollikainen, N., Quinodoz, S.A., Loney, C., Thai, J., Miller, Z.D., Lin, A.E., Schmidt, M.M., Stewart, D.G., Goldfarb, D., De Lorenzo, G., Rihn, S.J., Voorhees, R.M., Botten, J.W., Majumdar, D., and Guttman, M. (2020). SARS-CoV-2 Disrupts Splicing, Translation, and Protein Trafficking to Suppress Host Defenses. *Cell* 183**,** 1325-1339.e1321.

Bastard, P., Rosen, L.B., Zhang, Q., Michailidis, E., Hoffmann, H.H., Zhang, Y., Dorgham, K., Philippot, Q., Rosain, J., Béziat, V., Manry, J., Shaw, E., Haljasmägi, L., Peterson, P., Lorenzo, L., Bizien, L., Trouillet-Assant, S., Dobbs, K., De Jesus, A.A., Belot, A., Kallaste, A., Catherinot, E., Tandjaoui-Lambiotte, Y., Le Pen, J., Kerner, G., Bigio, B., Seeleuthner,

Y., Yang, R., Bolze, A., Spaan, A.N., Delmonte, O.M., Abers, M.S., Aiuti, A., Casari, G., Lampasona, V., Piemonti, L., Ciceri, F., Bilguvar, K., Lifton, R.P., Vasse, M., Smadja, D.M., Migaud, M., Hadjadj, J., Terrier, B., Duffy, D., Quintana-Murci, L., Van De Beek, D., Roussel, L., Vinh, D.C., Tangye, S.G., Haerynck, F., Dalmau, D., Martinez-Picado, J., Brodin, P., Nussenzweig, M.C., Boisson-Dupuis, S., Rodríguez-Gallego, C., Vogt, G., Mogensen, T.H., Oler, A.J., Gu, J., Burbelo, P.D., Cohen, J.I., Biondi, A., Bettini, L.R., D'angio, M., Bonfanti, P., Rossignol, P., Mayaux, J., Rieux-Laucat, F., Husebye, E.S., Fusco, F., Ursini, M.V., Imberti, L., Sottini, A., Paghera, S., Quiros-Roldan, E., Rossi, C., Castagnoli, R., Montagna, D., Licari, A., Marseglia, G.L., Duval, X., Ghosn, J., Tsang, J.S., Goldbach-Mansky, R., Kisand, K., Lionakis, M.S., Puel, A., Zhang, S.Y., Holland, S.M., Gorochov, G., Jouanguy, E., Rice, C.M., Cobat, A., Notarangelo, L.D., Abel, L., Su, H.C., and Casanova, J.L. (2020). Autoantibodies against type I IFNs in patients with life-threatening COVID-19. *Science* 370.

Beigel, J.H., Tomashek, K.M., Dodd, L.E., Mehta, A.K., Zingman, B.S., Kalil, A.C., Hohmann, E., Chu, H.Y., Luetkemeyer, A., Kline, S., Lopez De Castilla, D., Finberg, R.W., Dierberg, K., Tapson, V., Hsieh, L., Patterson, T.F., Paredes, R., Sweeney, D.A., Short, W.R., Touloumi, G., Lye, D.C., Ohmagari, N., Oh, M.-D., Ruiz-Palacios, G.M., Benfield, T., Fätkenheuer, G., Kortepeter, M.G., Atmar, R.L., Creech, C.B., Lundgren, J., Babiker, A.G., Pett, S., Neaton, J.D., Burgess, T.H., Bonnett, T., Green, M., Makowski, M., Osinusi, A., Nayak, S., and Lane, H.C. (2020). Remdesivir for the Treatment of Covid-19 — Final Report. *New England Journal of Medicine* 383**,** 1813-1826.

Blanco-Melo, D., Nilsson-Payant, B.E., Liu, W.C., Uhl, S., Hoagland, D., Møller, R., Jordan, T.X., Oishi, K., Panis, M., Sachs, D., Wang, T.T., Schwartz, R.E., Lim, J.K., Albrecht, R.A., and Tenoever, B.R. (2020). Imbalanced Host Response to SARS-CoV-2 Drives Development of COVID-19. *Cell* 181**,** 1036-1045.e1039.

Boni, M.F., Lemey, P., Jiang, X., Lam, T.T., Perry, B.W., Castoe, T.A., Rambaut, A., and Robertson, D.L. (2020). Evolutionary origins of the SARS-CoV-2 sarbecovirus lineage responsible for the COVID-19 pandemic. *Nat Microbiol* 5**,** 1408-1417.

Bost, P., Giladi, A., Liu, Y., Bendjelal, Y., Xu, G., David, E., Blecher-Gonen, R., Cohen, M., Medaglia, C., Li, H., Deczkowska, A., Zhang, S., Schwikowski, B., Zhang, Z., and Amit, I. (2020). Host-Viral Infection Maps Reveal Signatures of Severe COVID-19 Patients. *Cell* 181**,** 1475-1488.e1412.

Brisse, M., and Ly, H. (2019). Comparative Structure and Function Analysis of the RIG-I-Like Receptors: RIG-I and MDA5. *Frontiers in Immunology* 10.

Bronte, V., Ugel, S., Tinazzi, E., Vella, A., De Sanctis, F., Canè, S., Batani, V., Trovato, R., Fiore, A., Petrova, V., Hofer, F., Barouni, R.M., Musiu, C., Caligola, S., Pinton, L., Torroni, L., Polati, E., Donadello, K., Friso, S., Pizzolo, F., Iezzi, M., Facciotti, F., Pelicci, P.G., Righetti, D., Bazzoni, P., Rampudda, M., Comel, A., Mosaner, W., Lunardi, C., and Olivieri, O. (2020). Baricitinib restrains the immune dysregulation in patients with severe COVID-19. *J Clin Invest* 130**,** 6409-6416.

Chua, R.L., Lukassen, S., Trump, S., Hennig, B.P., Wendisch, D., Pott, F., Debnath, O., Thürmann, L., Kurth, F., Völker, M.T., Kazmierski, J., Timmermann, B., Twardziok, S., Schneider, S., Machleidt, F., Müller-Redetzky, H., Maier, M., Krannich, A., Schmidt, S., Balzer, F., Liebig, J., Loske, J., Suttorp, N., Eils, J., Ishaque, N., Liebert, U.G., Von Kalle, C., Hocke, A.,

Witzenrath, M., Goffinet, C., Drosten, C., Laudi, S., Lehmann, I., Conrad, C., Sander, L.E., and Eils, R. (2020). COVID-19 severity correlates with airway epithelium-immune cell interactions identified by single-cell analysis. *Nat Biotechnol* 38**,** 970-979.

Corman, V.M., Landt, O., Kaiser, M., Molenkamp, R., Meijer, A., Chu, D.K., Bleicker, T., Brünink, S., Schneider, J., Schmidt, M.L., Mulders, D.G., Haagmans, B.L., Van Der Veer, B., Van Den Brink, S., Wijsman, L., Goderski, G., Romette, J.-L., Ellis, J., Zambon, M., Peiris, M., Goossens, H., Reusken, C., Koopmans, M.P., and Drosten, C. (2020). Detection of 2019 novel coronavirus (2019-nCoV) by real-time RT-PCR. *Euro surveillance : bulletin Europeen sur les maladies transmissibles = European communicable disease bulletin* 25**,** 2000045.

Davidson, A.D., Williamson, M.K., Lewis, S., Shoemark, D., Carroll, M.W., Heesom, K.J., Zambon, M., Ellis, J., Lewis, P.A., Hiscox, J.A., and Matthews, D.A. (2020). Characterisation of the transcriptome and proteome of SARS-CoV-2 reveals a cell passage induced in-frame deletion of the furin-like cleavage site from the spike glycoprotein. *Genome Med* 12**,** 68.

Docherty, A.B., Harrison, E.M., Green, C.A., Hardwick, H.E., Pius, R., Norman, L., Holden, K.A., Read, J.M., Dondelinger, F., Carson, G., Merson, L., Lee, J., Plotkin, D., Sigfrid, L., Halpin, S., Jackson, C., Gamble, C., Horby, P.W., Nguyen-Van-Tam, J.S., Ho, A., Russell, C.D., Dunning, J., Openshaw, P.J., Baillie, J.K., and Semple, M.G. (2020). Features of 20 133 UK patients in hospital with covid-19 using the ISARIC WHO Clinical Characterisation Protocol: prospective observational cohort study. *Bmj* 369**,** m1985.

Eastman, R.T., Roth, J.S., Brimacombe, K.R., Simeonov, A., Shen, M., Patnaik, S., and Hall, M.D. (2020). Remdesivir: A Review of Its Discovery and Development Leading to Emergency Use Authorization for Treatment of COVID-19. *ACS Cent Sci* 6**,** 672-683.

Giamarellos-Bourboulis, E.J., Netea, M.G., Rovina, N., Akinosoglou, K., Antoniadou, A., Antonakos, N., Damoraki, G., Gkavogianni, T., Adami, M.E., Katsaounou, P., Ntaganou, M., Kyriakopoulou, M., Dimopoulos, G., Koutsodimitropoulos, I., Velissaris, D., Koufargyris, P., Karageorgos, A., Katrini, K., Lekakis, V., Lupse, M., Kotsaki, A., Renieris, G., Theodoulou, D., Panou, V., Koukaki, E., Koulouris, N., Gogos, C., and Koutsoukou, A. (2020). Complex Immune Dysregulation in COVID-19 Patients with Severe Respiratory Failure. *Cell Host Microbe* 27**,** 992-1000.e1003.

Hoang, T.N., Pino, M., Boddapati, A.K., Viox, E.G., Starke, C.E., Upadhyay, A.A., Gumber, S., Nekorchuk, M., Busman-Sahay, K., Strongin, Z., Harper, J.L., Tharp, G.K., Pellegrini, K.L., Kirejczyk, S., Zandi, K., Tao, S., Horton, T.R., Beagle, E.N., Mahar, E.A., Lee, M.Y.H., Cohen, J., Jean, S.M., Wood, J.S., Connor-Stroud, F., Stammen, R.L., Delmas, O.M., Wang, S., Cooney, K.A., Sayegh, M.N., Wang, L., Filev, P.D., Weiskopf, D., Silvestri, G., Waggoner, J., Piantadosi, A., Kasturi, S.P., Al-Shakhshir, H., Ribeiro, S.P., Sekaly, R.P., Levit, R.D., Estes, J.D., Vanderford, T.H., Schinazi, R.F., Bosinger, S.E., and Paiardini, M. (2020). Baricitinib treatment resolves lower-airway macrophage inflammation and neutrophil recruitment in SARS-CoV-2-infected rhesus macaques. *Cell*.

Hoffmann, M., Kleine-Weber, H., Schroeder, S., Krüger, N., Herrler, T., Erichsen, S., Schiergens, T.S., Herrler, G., Wu, N.H., Nitsche, A., Müller, M.A., Drosten, C., and Pöhlmann, S. (2020). SARS-CoV-2 Cell Entry Depends on ACE2 and TMPRSS2 and Is Blocked by a Clinically Proven Protease Inhibitor. *Cell* 181**,** 271-280.e278.

Hornung, V., Ellegast, J., Kim, S., Brzózka, K., Jung, A., Kato, H., Poeck, H., Akira, S., Conzelmann, K.K., Schlee, M., Endres, S., and Hartmann, G. (2006). 5'-Triphosphate RNA is the ligand for RIG-I. *Science* 314**,** 994-997.

Kato, H., Takeuchi, O., Sato, S., Yoneyama, M., Yamamoto, M., Matsui, K., Uematsu, S., Jung, A., Kawai, T., Ishii, K.J., Yamaguchi, O., Otsu, K., Tsujimura, T., Koh, C.S., Reis E Sousa, C., Matsuura, Y., Fujita, T., and Akira, S. (2006). Differential roles of MDA5 and RIG-I helicases in the recognition of RNA viruses. *Nature* 441**,** 101-105.

Kim, K., Dauphin, A., Komurlu, S., Mccauley, S.M., Yurkovetskiy, L., Carbone, C., Diehl, W.E., Strambio-De-Castillia, C., Campbell, E.M., and Luban, J. (2019). Cyclophilin A protects HIV-1 from restriction by human TRIM5α. *Nat Microbiol* 4**,** 2044-2051.

Koopmans, M. (2020). SARS-CoV-2 and the human-animal interface: outbreaks on mink farms. *Lancet Infect Dis*.

Laing, A.G., Lorenc, A., Del Molino Del Barrio, I., Das, A., Fish, M., Monin, L., Muñoz-Ruiz, M., Mckenzie, D.R., Hayday, T.S., Francos-Quijorna, I., Kamdar, S., Joseph, M., Davies, D., Davis, R., Jennings, A., Zlatareva, I., Vantourout, P., Wu, Y., Sofra, V., Cano, F., Greco, M., Theodoridis, E., Freedman, J., Gee, S., Chan, J.N.E., Ryan, S., Bugallo-Blanco, E., Peterson, P., Kisand, K., Haljasmägi, L., Chadli, L., Moingeon, P., Martinez, L., Merrick, B., Bisnauthsing, K., Brooks, K., Ibrahim, M.a.A., Mason, J., Lopez Gomez, F., Babalola, K., Abdul-Jawad, S., Cason, J., Mant, C., Seow, J., Graham, C., Doores, K.J., Di Rosa, F., Edgeworth, J., Shankar-Hari, M., and Hayday, A.C. (2020). A dynamic COVID-19 immune signature includes associations with poor prognosis. *Nat Med* 26**,** 1623-1635.

Li, J., Liu, Y., and Zhang, X. (2010). Murine coronavirus induces type I interferon in oligodendrocytes through recognition by RIG-I and MDA5. *J Virol* 84**,** 6472-6482.

Li, Y., Renner, D.M., Comar, C.E., Whelan, J.N., Reyes, H.M., Cardenas-Diaz, F.L., Truitt, R., Tan, L.H., Dong, B., Alysandratos, K.D., Huang, J., Palmer, J.N., Adappa, N.D., Kohanski, M.A., Kotton, D.N., Silverman, R.H., Yang, W., Morrisey, E., Cohen, N.A., and Weiss, S.R. (2020). SARS-CoV-2 induces double-stranded RNA-mediated innate immune responses in respiratory epithelial derived cells and cardiomyocytes. *bioRxiv*.

Liao, M., Liu, Y., Yuan, J., Wen, Y., Xu, G., Zhao, J., Cheng, L., Li, J., Wang, X., Wang, F., Liu, L., Amit, I., Zhang, S., and Zhang, Z. (2020). Single-cell landscape of bronchoalveolar immune cells in patients with COVID-19. *Nature Medicine* 26**,** 842-844.

Lindenbach, B.D. (2009). Measuring HCV infectivity produced in cell culture and in vivo. *Methods Mol Biol* 510**,** 329-336.

Liu, G., Lee, J.H., Parker, Z.M., Acharya, D., Chiang, J.J., Van Gent, M., Riedl, W., Davis-Gardner, M.E., Wies, E., Chiang, C., and Gack, M.U. (2020). ISG15-dependent Activation of the RNA Sensor MDA5 and its Antagonism by the SARS-CoV-2 papain-like protease. *bioRxiv*.

Lucas, C., Wong, P., Klein, J., Castro, T.B.R., Silva, J., Sundaram, M., Ellingson, M.K., Mao, T., Oh, J.E., Israelow, B., Takahashi, T., Tokuyama, M., Lu, P., Venkataraman, A., Park, A., Mohanty, S., Wang, H., Wyllie, A.L., Vogels, C.B.F., Earnest, R., Lapidus, S., Ott, I.M., Moore, A.J., Muenker, M.C., Fournier, J.B., Campbell, M., Odio, C.D., Casanovas-Massana, A., Herbst, R., Shaw, A.C., Medzhitov, R., Schulz, W.L., Grubaugh, N.D., Dela Cruz, C., Farhadian, S., Ko, A.I., Omer, S.B., and Iwasaki, A. (2020). Longitudinal analyses reveal immunological misfiring in severe COVID-19. *Nature* 584**,** 463-469.

Mahase, E. (2020). Covid-19: Anti-TNF drug adalimumab to be trialled for patients in the community. *BMJ* 371**,** m3847.

Mehra, M.R., Desai, S.S., Kuy, S., Henry, T.D., and Patel, A.N. (2020). Cardiovascular Disease, Drug Therapy, and Mortality in Covid-19. *New England Journal of Medicine* 382**,** e102.

Miorin, L., Kehrer, T., Sanchez-Aparicio, M.T., Zhang, K., Cohen, P., Patel, R.S., Cupic, A., Makio, T., Mei, M., Moreno, E., Danziger, O., White, K.M., Rathnasinghe, R., Uccellini, M., Gao, S., Aydillo, T., Mena, I., Yin, X., Martin-Sancho, L., Krogan, N.J., Chanda, S.K., Schotsaert, M., Wozniak, R.W., Ren, Y., Rosenberg, B.R., Fontoura, B.M.A., and García-Sastre, A. (2020). SARS-CoV-2 Orf6 hijacks Nup98 to block STAT nuclear import and antagonize interferon signaling. *Proc Natl Acad Sci U S A* 117**,** 28344-28354.

Nicholls, J.M., Poon, L.L., Lee, K.C., Ng, W.F., Lai, S.T., Leung, C.Y., Chu, C.M., Hui, P.K., Mak, K.L., Lim, W., Yan, K.W., Chan, K.H., Tsang, N.C., Guan, Y., Yuen, K.Y., and Peiris, J.S. (2003). Lung pathology of fatal severe acute respiratory syndrome. *Lancet* 361**,** 1773-1778.

Ogando, N.S., Dalebout, T.J., Zevenhoven-Dobbe, J.C., Limpens, R., Van Der Meer, Y., Caly, L., Druce, J., De Vries, J.J.C., Kikkert, M., Bárcena, M., Sidorov, I., and Snijder, E.J. (2020). SARS-coronavirus-2 replication in Vero E6 cells: replication kinetics, rapid adaptation and cytopathology. *J Gen Virol* 101**,** 925-940.

Pairo-Castineira, E., Clohisey, S., Klaric, L., Bretherick, A.D., Rawlik, K., Pasko, D., Walker, S., Parkinson, N., Fourman, M.H., Russell, C.D., Furniss, J., Richmond, A., Gountouna, E., Wrobel, N., Harrison, D., Wang, B., Wu, Y., Meynert, A., Griffiths, F., Oosthuyzen, W., Kousathanas, A., Moutsianas, L., Yang, Z., Zhai, R., Zheng, C., Grimes, G., Beale, R., Millar, J., Shih, B., Keating, S., Zechner, M., Haley, C., Porteous, D.J., Hayward, C., Yang, J., Knight, J., Summers, C., Shankar-Hari, M., Klenerman, P., Turtle, L., Ho, A., Moore, S.C., Hinds, C., Horby, P., Nichol, A., Maslove, D., Ling, L., Mcauley, D., Montgomery, H., Walsh, T., Pereira, A., Renieri, A., Millar, J., Nichol, A., Walsh, T., Openshaw, P.J.M., Shankar-Hari, M., Ponting, C., Meikle, J., Finernan, P., Mcmaster, E., Law, A., Baillie, J.K., Paterson, T., Wackett, T., Armstrong, R., Clark, R., Coutts, A., Donnelly, L., Gilchrist, T., Hafezi, K., Macgillivray, L., Maclean, A., Mccafferty, S., Morrice, K., Weaver, J., Boz, C., Golightly, A., Ward, M., Mal, H., Szoor-Mcelhinney, H., Brown, A., Hendry, R., Stenhouse, A., Cullum, L., Law, D., Law, S., Law, R., Swets, M., Day, N., Taneski, F., Duncan, E., Parkinson, N., Collier, D., Wood, S., Zak, A., Borra, C., Matharu, M., May, P., Alldis, Z., et al. (2020). Genetic mechanisms of critical illness in Covid-19. *Nature*.

Paranjpe, I., Russak, A.J., De Freitas, J.K., Lala, A., Miotto, R., Vaid, A., Johnson, K.W., Danieletto, M., Golden, E., Meyer, D., Singh, M., Somani, S., Kapoor, A., O'hagan, R., Manna, S., Nangia, U., Jaladanki, S.K., O'reilly, P., Huckins, L.M., Glowe, P., Kia, A., Timsina, P., Freeman, R.M., Levin, M.A., Jhang, J., Firpo, A., Kovatch, P., Finkelstein, J., Aberg, J.A., Bagiella, E., Horowitz, C.R., Murphy, B., Fayad, Z.A., Narula, J., Nestler, E.J., Fuster, V., Cordon-Cardo, C., Charney, D., Reich, D.L., Just, A., Bottinger, E.P., Charney, A.W., Glicksberg, B.S., and Nadkarni, G.N. (2020). Retrospective cohort study of clinical characteristics of 2199 hospitalised patients with COVID-19 in New York City. *BMJ Open* 10**,** e040736.

Park, A., and Iwasaki, A. (2020). Type I and Type III Interferons - Induction, Signaling, Evasion, and Application to Combat COVID-19. *Cell Host Microbe* 27**,** 870-878.

Rasaiyaah, J., Tan, C.P., Fletcher, A.J., Price, A.J., Blondeau, C., Hilditch, L., Jacques, D.A., Selwood, D.L., James, L.C., Noursadeghi, M., and Towers, G.J. (2013). HIV-1 evades innate immune recognition through specific cofactor recruitment. *Nature* 503**,** 402-405.

Rebendenne, A., Chaves, A., Tauziet, M., Maarifi, G., Bonaventure, B., Planès, R., Mckellar, J., Nisole, S., Arnaud-Arnould, M., Moncorgé, O., and Goujon, C. (2020). SARS-CoV-2 replication triggers an MDA-5-dependent interferon production which is unable to efficiently control replication. *bioRxiv***,** 2020.2010.2028.358945.

Reed, L.J.M., H (1938). A simple method of estimating fifty percent end points. *Am. J. Hyg.* 27**,** 493-497.

Rehwinkel, J., Tan, C.P., Goubau, D., Schulz, O., Pichlmair, A., Bier, K., Robb, N., Vreede, F., Barclay, W., Fodor, E., and Reis E Sousa, C. (2010). RIG-I detects viral genomic RNA during negative-strand RNA virus infection. *Cell* 140**,** 397-408.

Rodrigues, T.S., De Sá, K.S.G., Ishimoto, A.Y., Becerra, A., Oliveira, S., Almeida, L., Gonçalves, A.V., Perucello, D.B., Andrade, W.A., Castro, R., Veras, F.P., Toller-Kawahisa, J.E., Nascimento, D.C., De Lima, M.H.F., Silva, C.M.S., Caetite, D.B., Martins, R.B., Castro, I.A., Pontelli, M.C., De Barros, F.C., Do Amaral, N.B., Giannini, M.C., Bonjorno, L.P., Lopes, M.I.F., Santana, R.C., Vilar, F.C., Auxiliadora-Martins, M., Luppino-Assad, R., De Almeida, S.C.L., De Oliveira, F.R., Batah, S.S., Siyuan, L., Benatti, M.N., Cunha, T.M., Alves-Filho, J.C., Cunha, F.Q., Cunha, L.D., Frantz, F.G., Kohlsdorf, T., Fabro, A.T., Arruda, E., De Oliveira, R.D.R., Louzada-Junior, P., and Zamboni, D.S. (2021). Inflammasomes are activated in response to SARS-CoV-2 infection and are associated with COVID-19 severity in patients. *J Exp Med* 218.

Roth-Cross, J.K., Bender, S.J., and Weiss, S.R. (2008). Murine coronavirus mouse hepatitis virus is recognized by MDA5 and induces type I interferon in brain macrophages/microglia. *J Virol* 82**,** 9829-9838.

Schindelin, J., Arganda-Carreras, I., Frise, E., Kaynig, V., Longair, M., Pietzsch, T., Preibisch, S., Rueden, C., Saalfeld, S., Schmid, B., Tinevez, J.Y., White, D.J., Hartenstein, V., Eliceiri, K., Tomancak, P., and Cardona, A. (2012). Fiji: an open-source platform for biological-image analysis. *Nat Methods* 9**,** 676-682.

Stanifer, M.L., Kee, C., Cortese, M., Zumaran, C.M., Triana, S., Mukenhirn, M., Kraeusslich, H.G., Alexandrov, T., Bartenschlager, R., and Boulant, S. (2020). Critical Role of Type III Interferon in Controlling SARS-CoV-2 Infection in Human Intestinal Epithelial Cells. *Cell Rep* 32**,** 107863.

Sumner, R.P., Harrison, L., Touizer, E., Peacock, T.P., Spencer, M., Zuliani-Alvarez, L., and Towers, G.J. (2020). Disrupting HIV-1 capsid formation causes cGAS sensing of viral DNA. *The EMBO journal* 39**,** e103958-e103958.

Sumner, R.P., Thorne, L.G., Fink, D.L., Khan, H., Milne, R.S., and Towers, G.J. (2017). Are Evolution and the Intracellular Innate Immune System Key Determinants in HIV Transmission? *Frontiers in immunology* 8**,** 1246-1246.

Szabo, P.A., Dogra, P., Gray, J.I., Wells, S.B., Connors, T.J., Weisberg, S.P., Krupska, I., Matsumoto, R., Poon, M.M.L., Idzikowski, E., Morris, S.E., Pasin, C., Yates, A.J., Ku, A., Chait, M., Davis-Porada, J., Zhou, J., Steinle, M., Mackay, S., Saqi, A., Baldwin, M., Sims, P.A., and Farber, D.L. (2020). Analysis of respiratory and systemic immune responses in COVID-19 reveals mechanisms of disease pathogenesis. *medRxiv*.

789 Totura, A.L., and Baric, R.S. (2012). SARS coronavirus pathogenesis: host innate immune
790 responses and viral antagonism of interferon. *Curr Opin Virol* 2**,** 264-275.
791 Treibel, T.A., Manisty, C., Burton, M., Mcknight, Á., Lambourne, J., Augusto, J.B., Couto-Parada,
792 X., Cutino-Moguel, T., Noursadeghi, M., and Moon, J.C. (2020). COVID-19: PCR screening
793 of asymptomatic health-care workers at London hospital. *Lancet* 395**,** 1608-1610.
794 Wang, L.F., and Eaton, B.T. (2007). Bats, civets and the emergence of SARS. *Curr Top Microbiol*
795 *Immunol* 315**,** 325-344.
796 Williamson, E.J., Walker, A.J., Bhaskaran, K., Bacon, S., Bates, C., Morton, C.E., Curtis, H.J.,
797 Mehrkar, A., Evans, D., Inglesby, P., Cockburn, J., Mcdonald, H.I., Mackenna, B.,
798 Tomlinson, L., Douglas, I.J., Rentsch, C.T., Mathur, R., Wong, A.Y.S., Grieve, R., Harrison,
799 D., Forbes, H., Schultze, A., Croker, R., Parry, J., Hester, F., Harper, S., Perera, R., Evans,
800 S.J.W., Smeeth, L., and Goldacre, B. (2020). Factors associated with COVID-19-related
801 death using OpenSAFELY. *Nature* 584**,** 430-436.
802 Wolff, D., Nee, S., Hickey, N.S., and Marschollek, M. (2020). Risk factors for Covid-19 severity
803 and fatality: a structured literature review. *Infection*.
804 Wu, B., Peisley, A., Richards, C., Yao, H., Zeng, X., Lin, C., Chu, F., Walz, T., and Hur, S. (2013).
805 Structural basis for dsRNA recognition, filament formation, and antiviral signal activation
806 by MDA5. *Cell* 152**,** 276-289.
807 Yuen, C.K., Lam, J.Y., Wong, W.M., Mak, L.F., Wang, X., Chu, H., Cai, J.P., Jin, D.Y., To, K.K., Chan,
808 J.F., Yuen, K.Y., and Kok, K.H. (2020). SARS-CoV-2 nsp13, nsp14, nsp15 and orf6 function
809 as potent interferon antagonists. *Emerg Microbes Infect* 9**,** 1418-1428.
810 Zang, R., Gomez Castro, M.F., Mccune, B.T., Zeng, Q., Rothlauf, P.W., Sonnek, N.M., Liu, Z.,
811 Brulois, K.F., Wang, X., Greenberg, H.B., Diamond, M.S., Ciorba, M.A., Whelan, S.P.J., and
812 Ding, S. (2020). TMPRSS2 and TMPRSS4 promote SARS-CoV-2 infection of human small
813 intestinal enterocytes. *Sci Immunol* 5.
814 Zhang, Q., Bastard, P., Liu, Z., Le Pen, J., Moncada-Velez, M., Chen, J., Ogishi, M., Sabli, I.K.D.,
815 Hodeib, S., Korol, C., Rosain, J., Bilguvar, K., Ye, J., Bolze, A., Bigio, B., Yang, R., Arias,
816 A.A., Zhou, Q., Zhang, Y., Onodi, F., Korniotis, S., Karpf, L., Philippot, Q., Chbihi, M.,
817 Bonnet-Madin, L., Dorgham, K., Smith, N., Schneider, W.M., Razooky, B.S., Hoffmann,
818 H.H., Michailidis, E., Moens, L., Han, J.E., Lorenzo, L., Bizien, L., Meade, P., Neehus, A.L.,
819 Ugurbil, A.C., Corneau, A., Kerner, G., Zhang, P., Rapaport, F., Seeleuthner, Y., Manry, J.,
820 Masson, C., Schmitt, Y., Schlüter, A., Le Voyer, T., Khan, T., Li, J., Fellay, J., Roussel, L.,
821 Shahrooei, M., Alosaimi, M.F., Mansouri, D., Al-Saud, H., Al-Mulla, F., Almourfi, F., Al-
822 Muhsen, S.Z., Alsohime, F., Al Turki, S., Hasanato, R., Van De Beek, D., Biondi, A., Bettini,
823 L.R., D'angio, M., Bonfanti, P., Imberti, L., Sottini, A., Paghera, S., Quiros-Roldan, E.,
824 Rossi, C., Oler, A.J., Tompkins, M.F., Alba, C., Vandernoot, I., Goffard, J.C., Smits, G.,
825 Migeotte, I., Haerynck, F., Soler-Palacin, P., Martin-Nalda, A., Colobran, R., Morange,
826 P.E., Keles, S., Çölkesen, F., Ozcelik, T., Yasar, K.K., Senoglu, S., Karabela Ş, N., Rodríguez-
827 Gallego, C., Novelli, G., Hraiech, S., Tandjaoui-Lambiotte, Y., Duval, X., Laouénan, C.,
828 Snow, A.L., Dalgard, C.L., Milner, J.D., Vinh, D.C., et al. (2020). Inborn errors of type I IFN
829 immunity in patients with life-threatening COVID-19. *Science* 370.
830 Zhou, F., Yu, T., Du, R., Fan, G., Liu, Y., Liu, Z., Xiang, J., Wang, Y., Song, B., Gu, X., Guan, L., Wei,
831 Y., Li, H., Wu, X., Xu, J., Tu, S., Zhang, Y., Chen, H., and Cao, B. (2020). Clinical course and

risk factors for mortality of adult inpatients with COVID-19 in Wuhan, China: a retrospective cohort study. *Lancet* 395**,** 1054-1062.

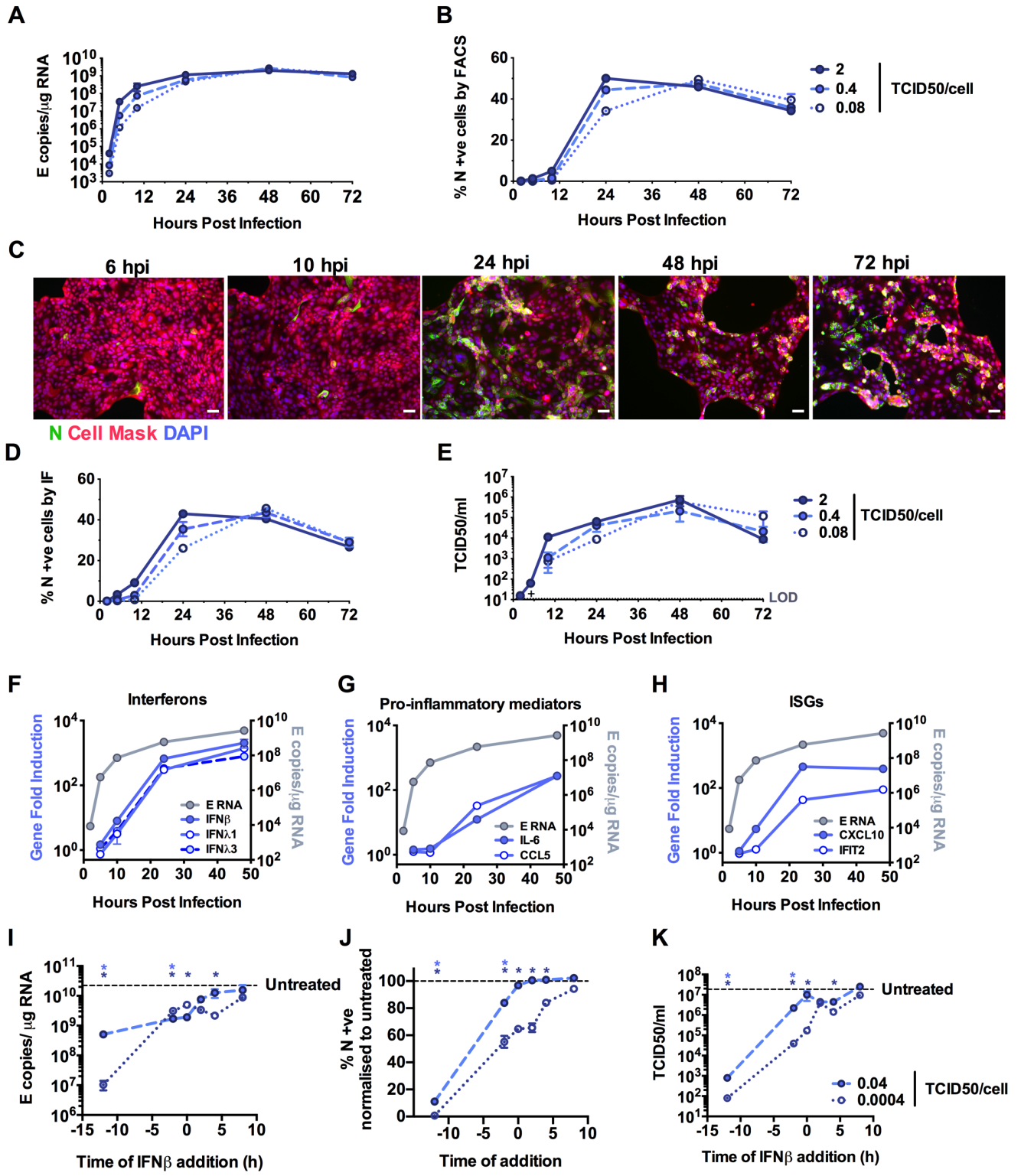

Figure 1.SARS-CoV-2 activates delayed innate immune responses in lung epithelial cells (**A-H**) Measurements of replication and innate immune induction in Calu-3 lung epithelial cells infected with SARS-CoV-2 at MOIs 0.08, 0.4 and 2 $TCID50_{VERO}$/cell. Means shown +/- SEM, n=2. (**A**) Replication of SARS-CoV-2 genomic and subgenomic E RNAs (qRT-PCR). (**B**) Quantification of N staining from cells in (A) by flow cytometry. Mean percentage of N-positive of all live-gated cells is shown +/- SEM, n=2. (**C**) Representative example of immunofluorescence staining of N protein (green) after SARS-CoV-2 infection of Calu-3 at MOI 0.4 $TCID50_{VERO}$/cell, at time points shown. Nuclei (DAPI, blue), cell mask (red). (**E**) Infectious virus released from cells in (A) determined by TCID50 on Vero.E6 cells, n=2. (**D**) Quantification of N staining in cells in (C) by immunofluorescence . (**E**) Infectious virus released from cells in (A) determined by TCID50 on Vero.E6 cells, n=2. (**F-H**) Fold induction of (**F**) interferons (IFNβ, IFNλ1 and IFNλ3) **(G)** IFN stimulated genes (CXCL10 and IFIT2) or **(H)** pro-inflammatory mediators (IL-6 and CCL5) each overlaid with SARS-CoV-2 E (qRT-PCR). All data from cells in (A) at MOI 0.4 $TCID50_{VERO}$/cell. Mean +/- SEM, n=2. (**I-L**) SARS-CoV-2 infection (MOIs 0.04 (closed symbols) and 0.0004 (open symbols) $TCID50_{VERO}$/cell) in Calu-3 cells with addition of 10ng/ml IFNβ before or after infection at time points shown, measured by **(I)** E RNA copies **(J)** N positive cells, **(L)** released virus ($TCID50_{VERO}$/cell) all measured at 24 hpi. Mean +/- SEM, n=3, One-way ANOVA Light and dark blue * indicates significance for high and low MOIs respectively.

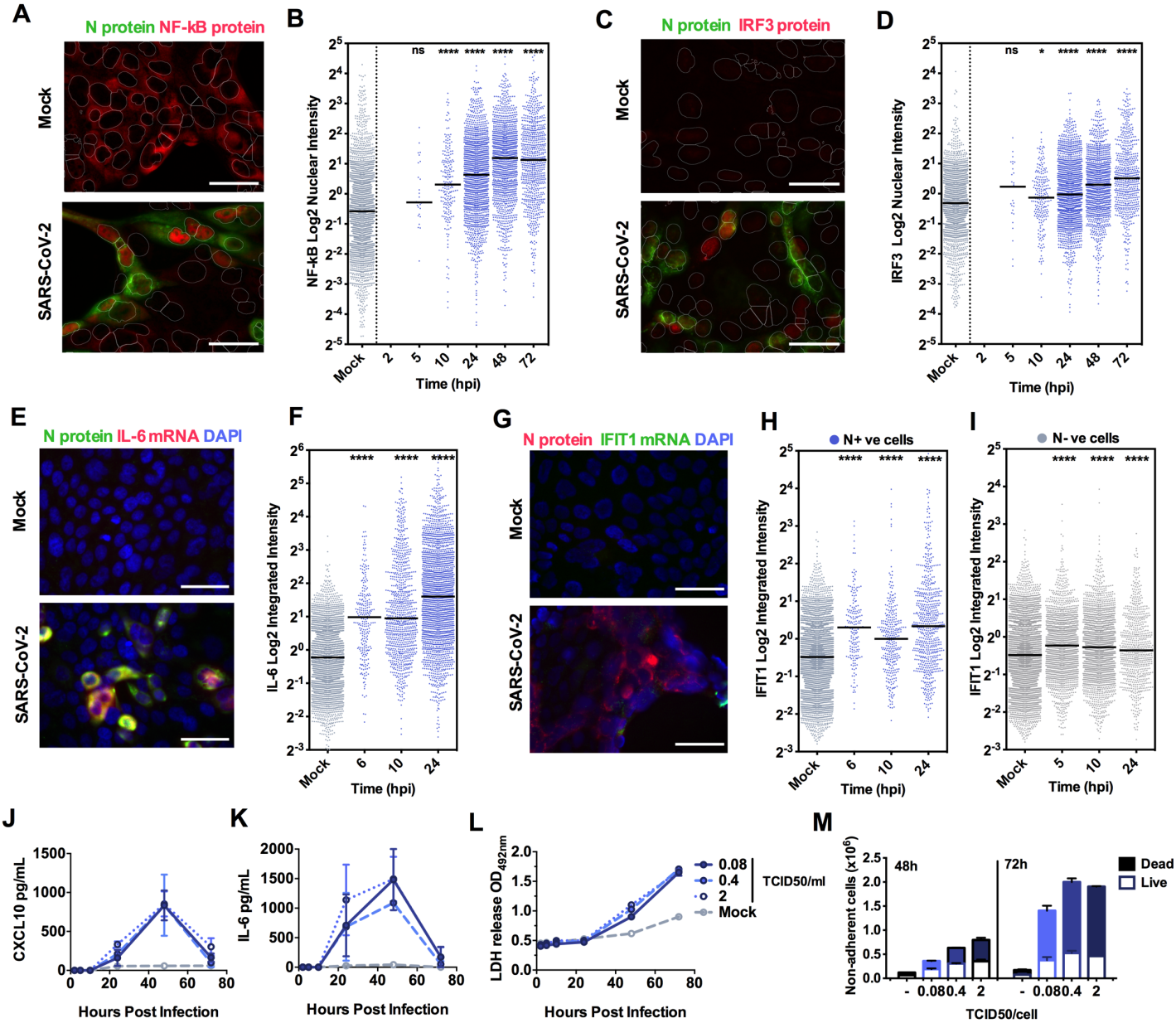

Figure 2. Peak SARS-CoV-2 replication precedes innate immune activation. (**A,C**) Representative images of NF-κB p65 (**A**) (red) and IRF3 (**C**) (red) nuclear localisation in mock or SARS-CoV-2 infected (MOI 0.4 $TCID50_{VERO}$/cell) Calu-3 cells at 24 hpi. SARS-CoV-2 N protein (green), nuclei (DAPI, blue). (**E and G**) Representative images of IL-6 mRNA (E) detected by FISH (red) and N protein (green) , or IFIT1 mRNA **(G)** (red) with N protein (green), both with nuclei (DAPI, blue) in mock or SARS-CoV-2 infected (MOI 0.4 $TCID50_{VERO}$/cell) Calu-3 cells at 24 hpi. **(B, D, F, H**) Single cell analysis time course quantifying the Integrated Nuclear Intensity of NF-κB p65 **(B),** IRF3 (**D**) , or overall integrated intensity for IL-6 **(F)** or IFIT1 **(H)** mRNA over time in N protein positive cells and N protein negative cells (E). n=2. Kruskal-Wallis test with Dunn's multiple comparison. * ($p<0.05$), **** ($p<0.0001$). (**I, J**) Secretion of CXCL10 (**I**) and IL-6 (**J**) by infected Calu-3 cells (MOIs 0.08, 0.4 and 2 $TCID50_{VERO}$/cell), (ELISA). Mean +/- SEM, n=2. (**K**) Lactate dehydrogenase (LDH) release into culture supernatants by mock and SARS-CoV-2 infected Calu-3 cells (MOIs 0.08, 0.4 and 2 $TCID_{VERO}50$/cell) quantified absorbance (492nm), means +/- SEM, n=2. **(L**) Quantification of live/dead staining of non-adherent cells recovered from supernatants of mock or SARS-CoV-2 infected Calu-3 cultures at 48 and 72hpi. Mean +/- SEM (n=2).

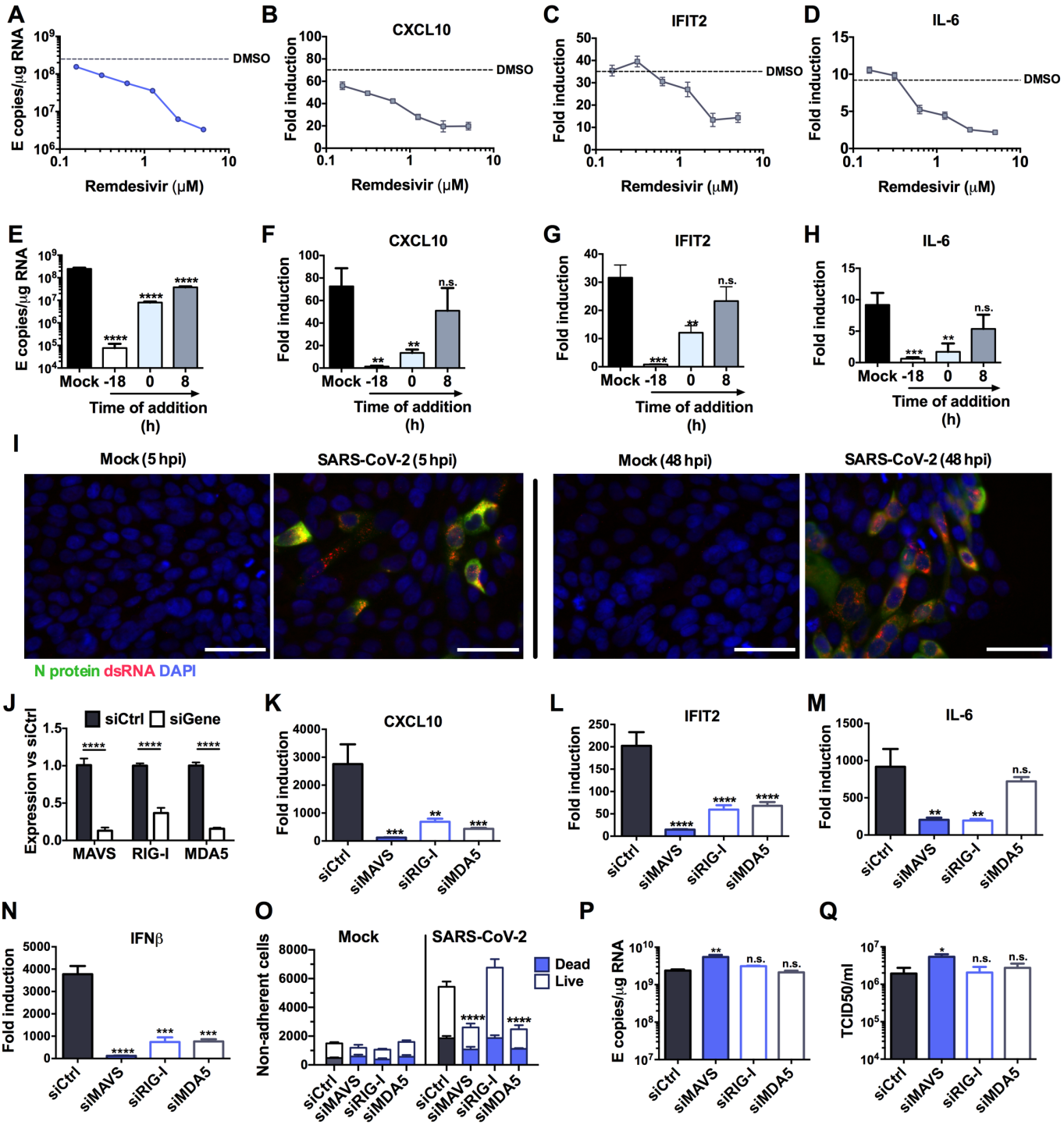

Figure 3. SARS-CoV-2 is sensed by MDA5 and RIG-I. (A-D) Measurement of (**A**) viral genomic and subgenomic E RNA at 24 hpi, (**B**) fold induction of CXCL10 from (A), (**C**) IFIT2 and (**D**) IL-6 mRNA (qRT-PCR) from (A) after Remdesivir treatment (0.125-5 µM) of SARS-CoV-2 infected Calu-3 cells (MOI 0.04 TCID50/cell) with Remdesivir added 2h prior to infection. Mean +/- SEM, n=3. (**E-H**) Measurement of (**E**) viral genomic and subgenomic E RNA (**F**) fold induction of CXCL10, **(G)** IFIT2, (**H**) and IL-6 at 24 hpi, of Calu-3 cells with SARS-CoV-2 (MOI 0.04 $TCID50_{VERO}$/cell) with Remdesivir treatment (5µM) prior to, at the time of, or 8 h post-infection. Mean +/- SEM, n=3, One way ANOVA with Dunnett's multiple comparisons test to compare to untreated infected condition ('mock'), ** (p<0.01), *** (p<0.001), **** (p<0.0001). (**I**) Representative example of immunofluorescence staining of dsRNA (red) and N protein (green) after SARS-CoV-2 infection of Calu-3 at MOI 0.4 $TCID50_{VERO}$/cell, at time points shown. Nuclei (DAPI, blue). **(J)** RNAi mediated depletion of MAVS, RIG-I or MDA-5, reduced their expression levels as compared to siControl (siCtrl) Mean +/- SEM. Two-Way ANOVA with Sidak's multiple comparisons test, **** (p<0.0001). (**K-N**) Fold induction of (**K**) CXCL10, (**L**) IFIT2, (**M**) IL-6 or (**N**) IFNβ in SARS-CoV-2 infected Calu-3 cells (MOI 0.04 TCID50/cell) 24 hpi. Mean +/- SEM, n=3, and compared to siCtrl for each gene by One Way ANOVA with Dunnett's multiple comparisons test, ** (p<0.01), *** (p<0.001), **** (p<0.0001), n.s. : non significant. (**O**) Live/dead stain counts for non-adherent cells, recovered at 48 hpi from supernatants of SARS-CoV-2 infected Calu-3 cells, depleted for MAVS, compared to siCtrl. Mean +/-SEM, n=3. Total numbers are compared to siCtrl by unpaired t-test, *** (p<0.001). Cell counts were determined by acquisition by flowcytometry for a defined period of time. Dead cells were determined by live/dead staining, means shown +/- SEM (n=3). (**P-Q**) (**P**) Viral E RNA and (**Q**) released infectious virus ($TCID50_{VERO}$/cell) at 24 hpi of infected Calu-3 cells depleted for MAVs, RIG-I or MDA5. Mean +/- SEM, n=3. Each group compared to siCtrl by One Way ANOVA with Dunnett's multiple comparisons test, *, p>0.05, ** (p<0.01), n.s : non significant.

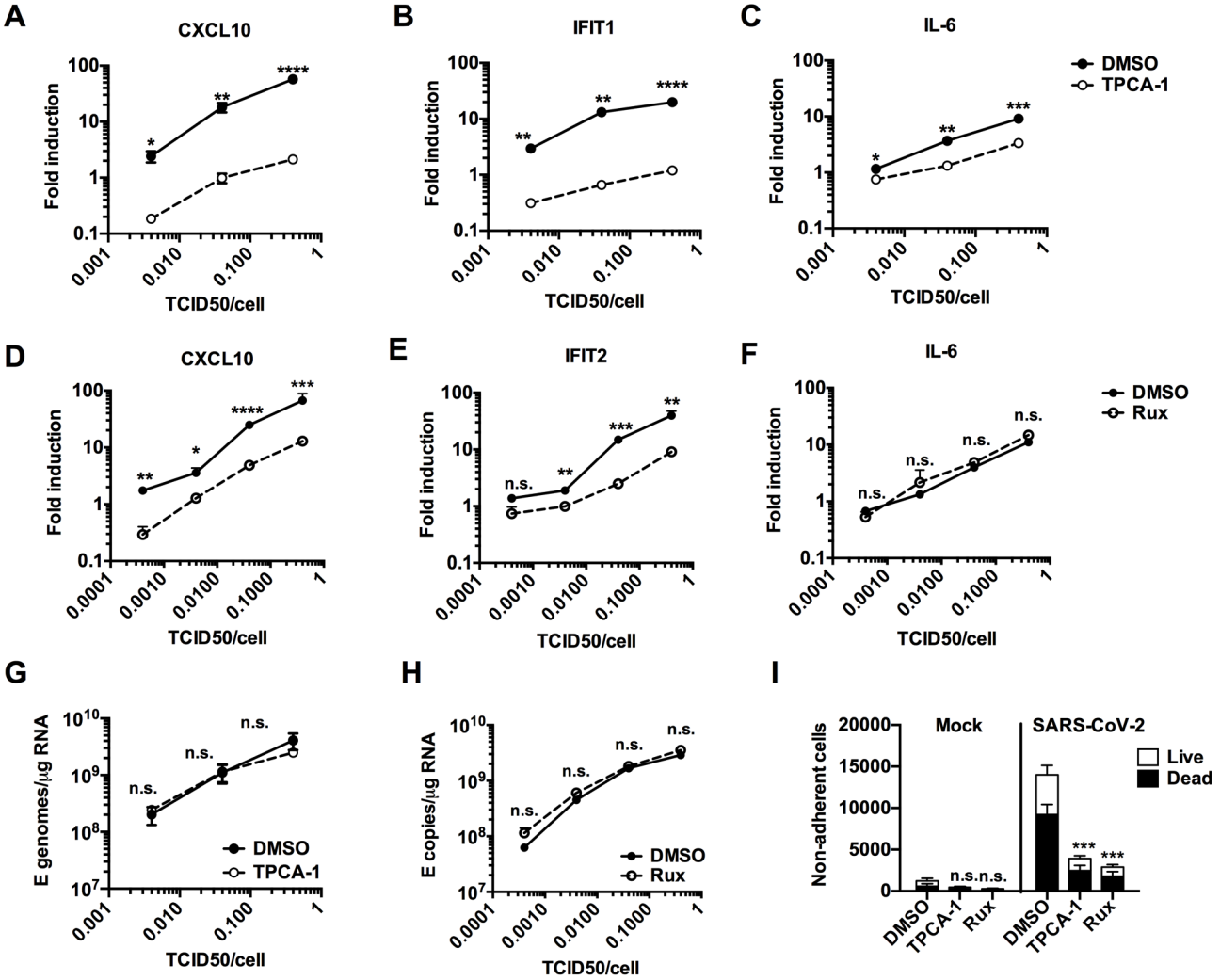

Figure 4. NF-kB and JAK/STAT signalling drive innate immune responses. (**A-C**) Fold induction at 24 hpi of (**A**) CXCL10, **(B)** IFIT1 or (**C**) IL-6 mRNA (qRT-PCR) after Calu-3 infection with SARS-CoV-2 over a range of MOIs (0.004, 0.04, 0.4 $TCID50_{VERO}$/cell) in the presence of 10 µM TPCA-1 or DMSO as shown. (**D-F**) Fold induction at 24 hpi of (**D**) CXCL10, **(E)** IFIT2 or (**F**) IL-6 mRNA (RT-qPCR) after Calu-3 infection with SARS-CoV-2 over a range of MOIs (0.0004, 0.004, 0.04, 0.4 $TCID50_{VERO}$/cell) in the presence of 2 µM Ruxolitinib (Rux) or DMSO as shown. (**G-H**) Viral genomic and subgenomic E RNA at 24 hpi (RT-qPCR) with DMSO or TPCA (G) or Rux (H) treatment. (A-H) Mean +/- SEM, n=3, (**A-H**) Statistical comparisons are made by unpaired t test comparing inhibitor-treated to mock-treated SARS-CoV-2 infected conditions at each MOI and each timepoint. * ($p<0.05$), ** ($p<0.01$), *** ($p<0.001$), **** ($p<0.0001$). (**I**) Live/dead stain count from non-adherent cells recovered from supernatants of SARS-CoV-2 infected Calu-3 cultures (MOI 0.04 $TCID50_{VERO}$/cell) 48hpi (flow cytometry). (n=3) One Way ANOVA comparison of inhibitor-treated infected cells to mock-treated infected cells. *** ($p<0.001$).

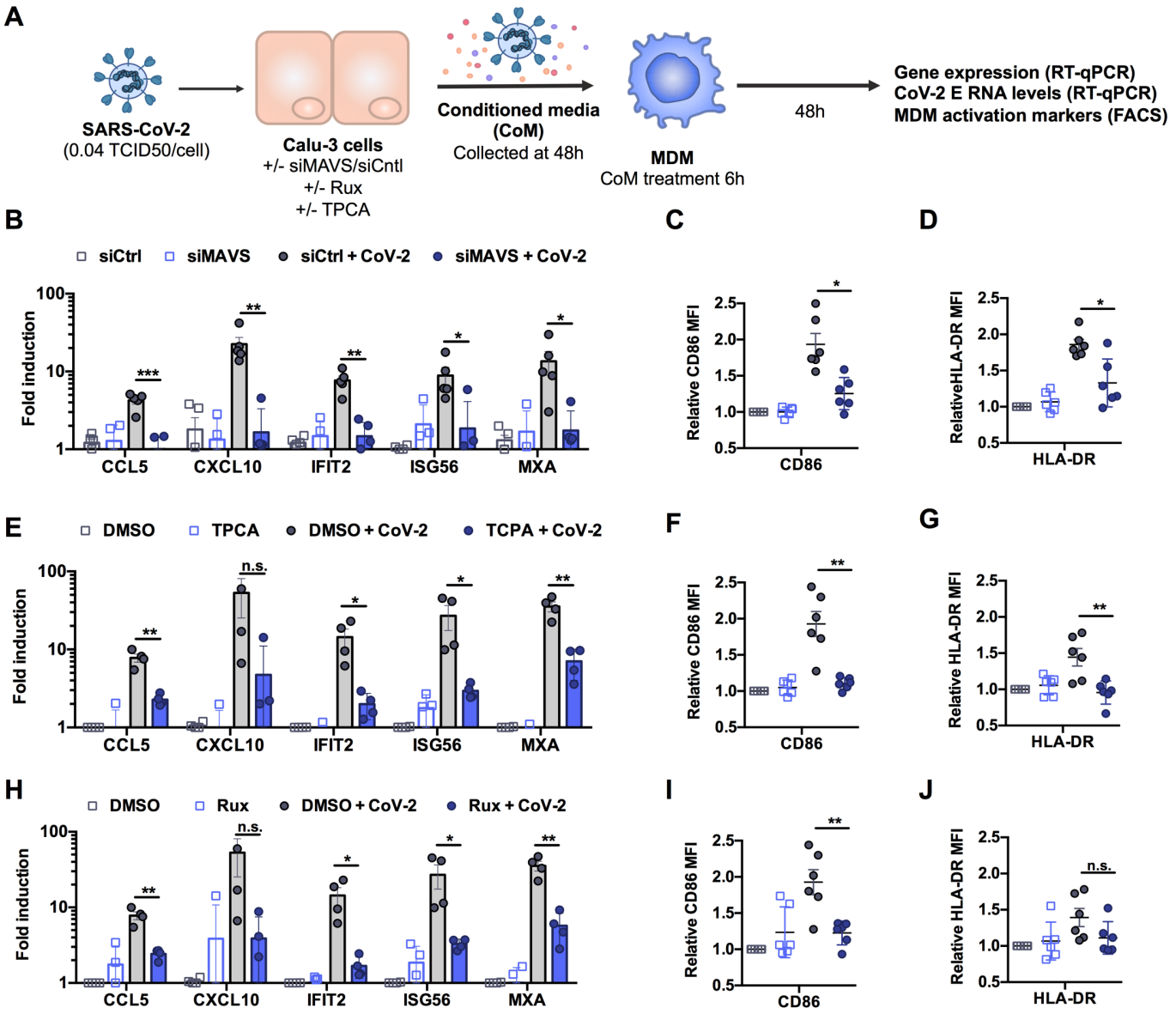

Figure 5. Epithelial responses to SARS-CoV-2 drive macrophage activation (**A**). Schematic of experimental design. (**B-J**) Calu-3 cells were transfected with siRNA targeting MAVS or non-targeting control (siCtrl) (B-D) or treated with DMSO vehicle or inhibitors 10 µM TPCA-1 (E-G) or 2 µM Ruxolitinib (Rux) (H-J) as shown, and were mock-infected or infected with SARS-CoV-2 at MOI 0.04 $TCID50_{VERO}$/cell. Virus containing conditioned media (CoM) was harvested at 48 hpi. MDM were treated with Calu-3 virus containing CoM for 6 hpi, before washing and measuring MDM gene expression (B, E, H), and MDM activation markers by flowcytometry 48 h later (C,D,F,G,I,J) , plotting relative median fluorescent intensity (MFI) compared to mock-infected siCtrl (C, D) or mock-infected DMSO control (F, G, I, J). Legends in (B), (E) and (H) apply to (C,D), (F,G) and (I,J) respectively. Mean +/- SEM shown, data from 4-6 independent MDM donors is shown. Statistical comparison by two-tailed paired t-test comparing MDM exposed to control infected CoM to siMAVS/inhibitor treated infected CoM. * ($p<0.05$), ** ($p<0.01$), *** ($p<0.001$).

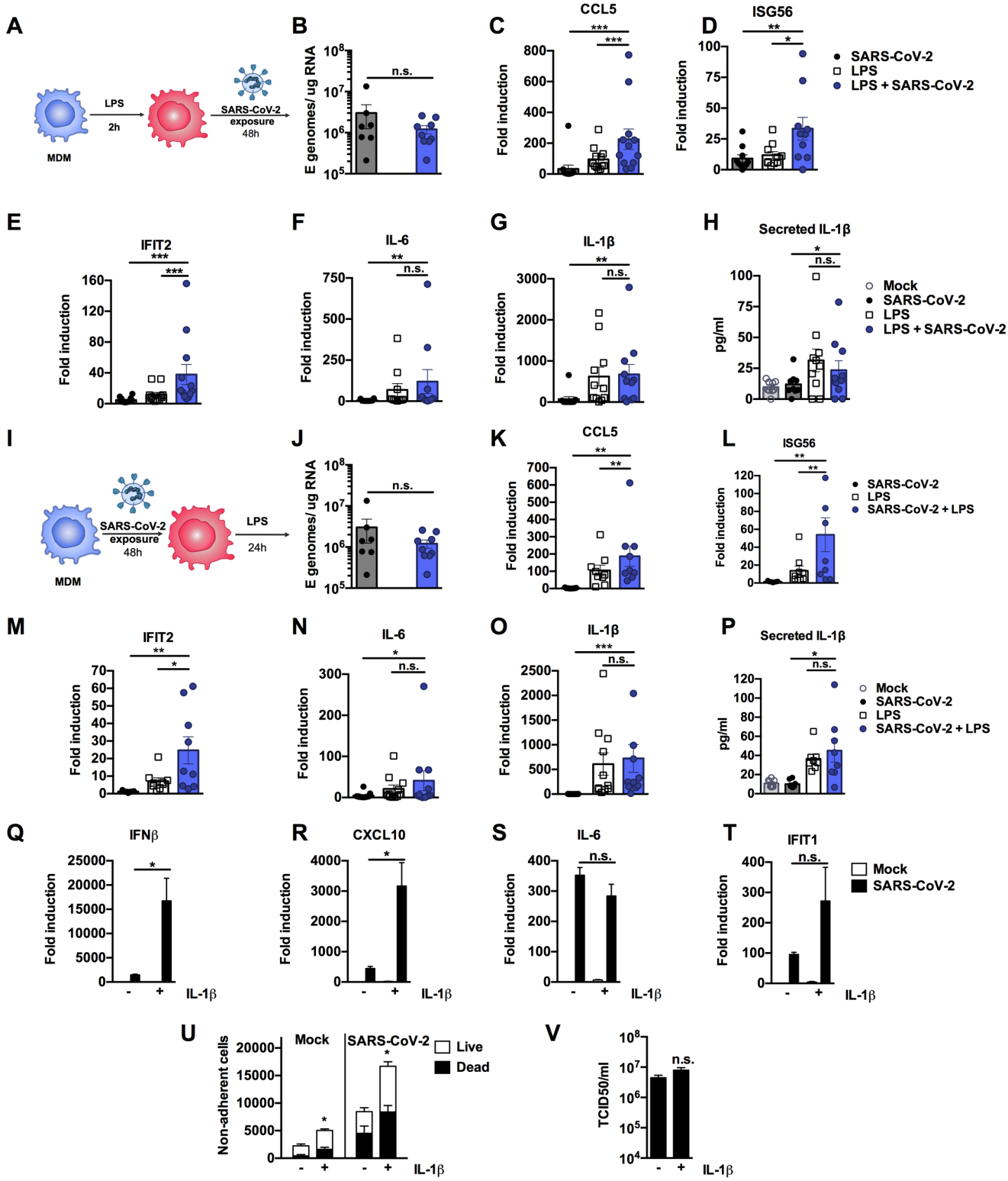

Figure 6. Pre-existing immune activation exacerbates SARS-CoV-2-dependent inflammation. (**A**) Schematic of experimental design. (**B-H**) MDM were primed with 100ng/ml LPS for 2h before exposure to SARS-CoV-2 (MOI 0.02 $TCID50_{VERO}$/cell). (**B**) Expression of genomic and subgenomic viral E RNA at 48 h post exposure in indicated conditions. (**C-G**) Host gene expression of (**C**) CCL5, (**D**) ISG56, (**E**) IFIT2, (**F**) IL-6 or (**G**) IL-1β was measured 48hpi. (**H**) IL-1β secretion was detected in culture supernatants at 48 hpi by ELISA. (**I**) Schematic of experimental design. MDM were exposed to SARS-CoV-2 (MOI 0.02 $TCID50_{VERO}$/cell) for 48 h and subsequently stimulated with 100ng/ml LPS for 24 h. (**J**) Expression of genomic and subgenomic viral E RNA 72 h post-exposure in indicated conditions. (**K-L**) Host gene expression of (**K**) CCL5, (**L**) ISG56), IFIT2 (**M**), (**N**) IL-6 and (**O**) IL-1β. (**P**) IL-1β secretion was detected in culture supernatants at 48 hpi by ELISA. Gene expression is shown as fold induction over untreated controls. Data from 8-13 independent donors is shown. Groups were compared as indicated by Wilcoxon matched-pairs signed rank test, *, $p<0.05$, ** ($p<0.01$), *** ($p<0.001$). (**Q-V**) Calu-3 cells were infected with SARS-CoV-2 (MOI 0.04 $TCID50_{VERO}$/cell) in the presence or absence of 10ng/ml IL-1β. (**Q-T**) Gene expression of (**Q**) IFNβ (**R**), CXCL10, (**S**) IL-6 and (**T**) IFIT1 was measured after 24h. Fold induction over untreated mock infection is shown, n=3. (**U**) Non-adherent cells were collected at 48h post infection and live/dead stained. Cells were acquired by flowcytometry and cell counts determined by time-gating. For statistical comparison, total cell numbers were compared. (**V**) Viral release into culture supernatants at 24 h was measured by TCID50 on VeroE6 cells. (**Q-V**) Mock and SARS-CoV-2 infected conditions were compared with or without IL1b-treatment, respectively, by unpaired T test (n=3). *, $p<0.05$; n.s., non-significant. Mean +/- SEM shown.